Zeitschrift: Helvetica Physica Acta
Band: 58 (1985)
Heft: 4

Artikel: Electronic and structural properties of single crystals in the system TiO_2-RuO_2
Autor: Triggs, P.
DOI: https://doi.org/10.5169/seals-115624

Helvetica Physica Acta, Vol. **58** (1985) 657–714

0018–0238/85/040657–58$1.50 + 0.20/0

Electronic and structural properties of single crystals in the system TiO_2–RuO_2

By P. Triggs[†])

Institut de Physique Appliquée, EPFL, CH-1015 Lausanne, Switzerland.

Abstract. We have studied single crystals in the TiO_2–RuO_2 system, grown by chemical vapour transport. The solubility limit of RuO_2 in TiO_2 is found to be 2–3 mol%, and is at least 2 mol% for TiO_2 in RuO_2. Crystals with intermediate compositions show a highly ordered microstructure with a Ti rich and a Ru rich phase. Titanium is found to scatter conduction electrons in RuO_2 but to have no apparent influence on the band structure. Ruthenium is shown to compensate both trivalent and pentavalent impurities in TiO_2, as well as point defects produced by reduction. All valence states from Ru^{5+} to Ru^{2+} have been observed in solid solution by Mössbauer spectroscopy or electron paramagnetic resonance. The optical and electrical properties of Ru doped TiO_2 have been studied, and allow the energy levels of the different valence states of ruthenium to be estimated.

Resume. Des monocristaux du système TiO_2–RuO_2, ont été obtenus par transport en phase vapeur. La limite de solubilité du RuO_2 dans le TiO_2 se situe entre 2 et 3 mol%. Elle est au moins superiéure à 2 mol% pour le TiO_2 dans le RuO_2. Les cristaux de composition intermédiaire présentent une microstructure ordonnée comprenant une phase riche de Ti et une phase riche de Ru. En solution solide dans le RuO_2, le titane produit des centres de diffusion des électrons de conduction, mais n'a pas d'influence apparente sur la structure de bande. Nous avons démontré que le ruthenium peut compenser des impurtés trivalentes et pentavalentes dans le TiO_2, de même que les défauts ponctuels créés par réduction. Tous les états de valence de Ru^{5+} à Ru^{2+} ont été observés en solution solide dans le TiO_2 par spectroscopie Mössbauer ou par résonance paramagnétique électronique. L'étude des propriété optiques et éléctriques du TiO_2 dopé au ruthénium a permis d'évaluer les énergies des différents états de valence du Ru.

Contents

[†]) Present address LGZ Landis & Gyr A. G, Zug, Switzerland.

1. Introduction

The intensive interest over the last decade in the TiO_2–RuO_2 system stems from the unique position of these two oxides, and their mixture in important electrochemical processes such as the production of hydrogen from water, and the production of chlorine. In this introduction we will give a short description of the method of hydrogen production by electrolysis of water showing the role which the TiO_2–RuO_2 system plays in this process. We will then introduce the main features of the work described in this report.

An electrolysis cell consists essentially of two electrodes immersed in an electrolyte, and connected to an external voltage supply. Application of a potential difference between the electrodes produces a current flow in the electrolyte with oxygen and hydrogen evolution at the anode and cathode respectively, the overall reaction being:

$$H_2O \rightarrow H_2 + \tfrac{1}{2}O_2 \qquad (1)$$

The cell voltage (U) required to drive the reaction is given by:

$$U = U^0 + \eta_a(i) + \eta_c(i) + Ri \tag{2}$$

where U^0 is the voltage corresponding to the free enthalpy change in reaction 1, η_a and η_c are the overvoltages at the anode and cathode respectively, R is the ohmic resistance of the cell, and i is the current. At room temperature U^0 is 1.23 V. The other contributions to the cell voltage result in energy loss, and must be minimised.

The ohmic resistance (R) depends on the bulk resistances of the cell components, especially the electrolyte, and can be minimised by optimising the cell design. The electrode overvoltages depend on the electrode materials used. Platinum is the best known catalyst for hydrogen evolution, and the overvoltage at a platinum cathode is only around 0.02 V at low current densities.

The choice of catalysts for the oxygen evolution reaction is limited to oxides, since no suitable metals are stable in the strongly oxidising conditions present at the anode. The oxide with the lowest overpotential for oxygen evolution is RuO_2. At room temperature and low current densities this has an overpotential of around 0.2 V which is about half the total overvoltage of a modern water electrolysis cell. Pure RuO_2 cannot be used as an electrode, however, for two reasons.

Firstly the corrosion rate of RuO_2 during oxygen evolution is very high and the service life of electrolysis cells depends essentially on the active life of the anode. Mixing with TiO_2 has been shown to stabilise RuO_2 electrodes for chlorine evolution [1], but for oxygen evolution, satisfactory stabilisation has only been achieved using IrO_2 [2].

Secondly the cost of ruthenium is too high for solid RuO_2 electrodes to be used. In most electrochemical applications the RuO_2 is diluted with a cheap, inert component, and the mixture is applied as a thin coating to a solid metal electrode. Although a number of inert oxides have been suggested, it is the TiO_2-RuO_2 mixture which is the most commonly used. Because of its low cost, lightness and relative chemical stability, titanium is the most frequently used metal for the electrode. This system is very successful as a chlorine evolution anode. A problem arises in the use of this electrode for oxygen evolution, however, in that slow oxidation of the titanium support occurs leading to an insulating TiO_2 layer under the active coating, and this may also shorten the useful life of the anode.

The combined problems of dilution and stabilisation against corrosion of the RuO_2 by TiO_2, and the passivation of the electrode by the formation of an insulating TiO_2 layer in contact with the RuO_2 film, have stimulated a large amount of pure and applied research on the TiO_2–RuO_2 system.

In parallel to the research on water electrolysis for hydrogen production, the photoelectrolytic decomposition of water has also attracted much attention in the last decade. Here again, attention has been drawn to the TiO_2–RuO_2 system, since fine dispersions of TiO_2 and RuO_2 are promising catalysers of this reaction [3].

Although attempts have been made to characterise the physical and chemical properties of the TiO_2–RuO_2 system, the samples used have always been relatively ill-defined, and the results obtained have varied significantly depending on the preparation techniques used [4]. For example, studies on RuO_2 single crystals

[2.5] have established without any doubt that RuO_2 is a good metal, but many early studies on RuO_2 films led to the conclusion that RuO_2 is a semiconductor. A contribution can therefore be made to our understanding of the TiO_2–RuO_2 system by studying single crystals, although up till now no growth technique applicable to both oxides was known.

The structure of this paper is as follows:

In Chapter two a short review of the electronic properties of pure, reduced and doped TiO_2 is given. The properties of RuO_2 are then discussed, and a review of recent studies on the TiO_2–RuO_2 system is given.

In Chapter three we describe the crystal growth program undertaken to prepare samples in the TiO_2–RuO_2 system.

In Chapter four we describe experiments on RuO_2 containing Ti, to determine the influence of Ti on the electronic properties of RuO_2.

The major part of the work presented here has been consecrated to the study of ruthenium doped titanium dioxide, and is presented in Chapter five. A number of experiments have been performed enabling a coherent picture of the role played by ruthenium as an impurity in TiO_2 to be developed.

In Section 5.1 we present a series of Mössbauer spectroscopy measurements on titanium dioxide doped with ruthenium, and both ruthenium and the donor tantalum. The spectra give information on the site occupied by the ruthenium ion, and on the electric field gradient present at that site. In addition it is possible to deduce the valence state of the ruthenium, and to observe changes in valence on addition of tantalum to the system.

In Section 5.2 we present electron paramagnetic resonance (EPR) measurements of ruthenium in TiO_2. Only ions in valence states with magnetic moments, in this case tri- and pentavalent ruthenium can be observed by this technique. It has been possible however to demonstrate changes in the valence state of the ruthenium on doping with tantalum in agreement with the Mössbauer measurements, and to show that changes also occur on reduction in hydrogen gas. It has further been possible to determine the spin hyperfine parameters of these ions, and to identify the sites on which they are located.

In Section 5.3 the optical absorption spectra of ruthenium doped TiO_2 are presented. The spectra obtained following reduction in vacuum and in hydrogen are given, and are compared to the spectra of TiO_2 doped with both ruthenium and tantalum. In the light of the Mössbauer and EPR studies it is possible to attribute the observed absorption bands to particular valence states of the ruthenium ion, and to deduce the optical transitions involved. This gives information on the energy levels of the various valence states with respect to the conduction and valence bands of titanium dioxide.

In Section 5.4 we give the results of electrical conductivity measurements on titanium dioxide samples doped with both ruthenium and tantalum. It is shown that ruthenium doped titanium dioxide is insulating, and that addition of tantalum increases appreciably the conductivity only after all the ruthenium is reduced to the divalent state.

In Section 5.5 photoelectron spectra of the valence and core levels of ruthenium doped TiO_2 are shown. The valence state of the ruthenium at the surface is shown to be different from that in the bulk as a result of downward band bending in the depletion zone.

The results of these studies are discussed in Section 5.6, and a model is

derived for the energy levels of ruthenium in TiO_2. In Section 6 we resume the principal results of this project.

This paper represents a slightly shortened version of the author's doctoral thesis. Certain results have been published elsewhere, but are included here for completeness.

2. Established properties of TiO_2, RuO_2, and mixed TiO_2–RuO_2 systems

2.1. Crystal structure

TiO_2 and RuO_2 belong to the family of transition metal dioxides which have the rutile structure as one of their structural modifications. RuO_2 has no other known phases whereas TiO_2 also exists in two less dense modifications, anatase, and brookite. These two phases are metastable derivatives of rutile, and convert to rutile on annealing. Most crystal growth techniques, including our own, yield directly the rutile phase, and it is for this reason that rutile is the most important and extensively studied of the three forms.

A striking diversity of electrical and magnetic properties is found within the family of rutile structure dioxides as shown in Table 2.1, taken from Mattheiss [5]. Within the 3d dioxides we find the wide band-gap semiconductor TiO_2, the Mott Transition of VO_2, the metallic ferromagnet CrO_2, and the antiferromagnetic semiconductor MnO_2. Less diversity is found in the 4d and 5d dioxides where apart from NbO_2 which shows a metal–semiconductor transition, the compounds are all metallic. Some of these have slightly distorted rutile structures with monoclinic or orthorhombic symmetry.

The two dioxides which interest us particularly in this study, TiO_2 and RuO_2 both have the undistorted tetragonal rutile structure.

The primitive unit cell for the rutile structure is shown in Fig. 2.1. Each unit cell contains two MO_2 molecules. The Bravais lattice is tetragonal with $c/a < 1$ in all known cases. The metal cations form a body centred tetragonal lattice and occupy the positions:

$(0, 0, 0)$ $(\frac{1}{2}, \frac{1}{2}, \frac{1}{2})$

The coordinates of the four oxygen anions in the unit cell are:

$(u, u, 0)$ $(1-u, 1-u, 0)$

$(\frac{1}{2}+u, \frac{1}{2}-u, \frac{1}{2})$ $(\frac{1}{2}-u, \frac{1}{2}+u, \frac{1}{2})$ where $u \approx 0.3$.

Table 2.1
Properties of transition metal dioxides with the rutile structure. Metals, semiconductors, ferromagnets and antiferromagnets are indicated by M, S, F, and AF, respectively.

	d^0	d^1	d^2	d^3	d^4	d^5	d^6
3d	TiO_2 (S)	VO_2^* (M–S)	CrO_2 (F–M)	MnO_2 (AF–S)			
4d		NbO_2^* (M–S)	MoO_2^* (M)	TcO_2^* (M)	RuO_2 (M)	RhO_2 (M)	
5d		TaO_2	WO_2^* (M)	ReO_2^* (M)	OsO_2 (M)	IrO_2 (M)	PtO_2^* (M)

*) Involves a distorted rutile structure.

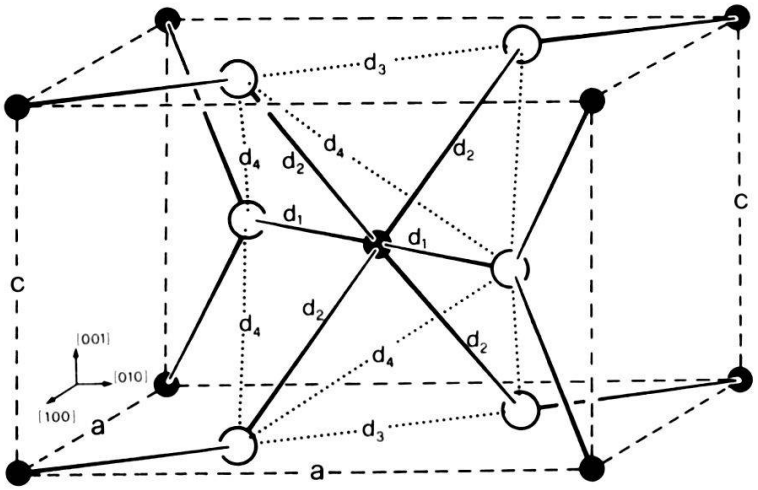

Figure 2.1
Unit cell of Rutile.

Each cation is surrounded by a distorted octahedron of six anions. The orientations of the octahedra surrounding adjacent cations differ by 90° rotations about the c axis. A summary of the lattice parameters and bondlengths is given for TiO_2 and RuO_2 in Table 2.2, using data from Baur and Khan [6].

The shortest cation–anion bonds in the structure may lie along the principal axis of the octahedron, [110], or in the (110) plane perpendicular to the principal axis, depending on c/a and u. In TiO_2 the twofold cation–anion bond along [110] is the shortest, while in RuO_2 the four bonds in the (110) plane are shorter.

One feature of the rutile structure is the existence of wide channels parallel to the c-axis and passing through the unit cell face centers. These channels give rise to extremely anisotropic diffusion for some impurity species, and lithium in TiO_2 has been found to diffuse at least 10^8 times faster parallel to the c-axis than perpendicular [7]. In these channels are found interstitial sites for impurity ions of both octahedral coordination (e.g. at $(\frac{1}{2}, 0, \frac{1}{2})$ and $(\frac{1}{2}, 0, 0)$) and tetrahedral coodination (e.g. at $(\frac{1}{2}, 0, \frac{1}{4})$ and $(\frac{1}{2}, 0, \frac{3}{4})$).

Table 2.2
Lattice parameters and bond lengths of RuO_2 and TiO_2.

Parameter	RuO_2	TiO_2
a(Å)	4.4919	4.594
c(Å)	3.1066	2.959
c/a	0.6916	0.6441
u	0.3058	0.3057
	Bond length (Å)	
M–M[001]	3.1066	2.959
[100]	4.4919	4.594
[111]	3.536	3.242
M–O d_1	1.942	1.986
d_2	1.984	1.945
O–O d_3	2.468	2.647
d_4	2.776	2.780

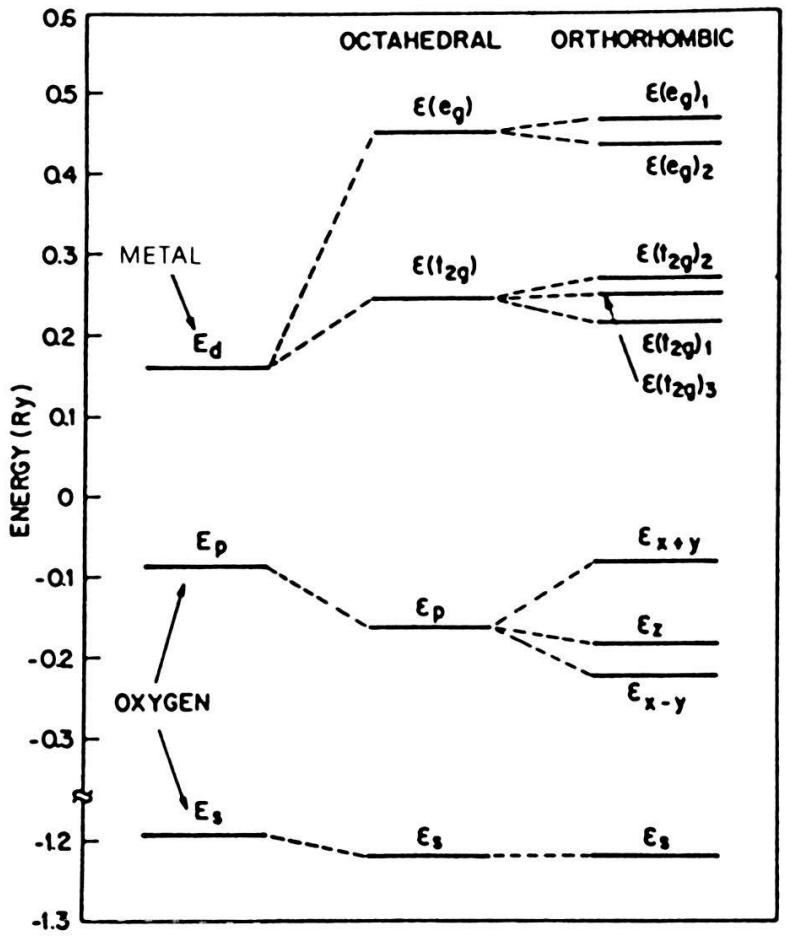

Figure 2.2
Ligand field splitting of metal d and oxygen 2p and 2s levels, first in an octahedral environment, then with an orthorhombic distortion as in the rutile structure, from Ref. 5.

The space group for the rutile structure is $D_{4h}^{14}(P4_2/mnm)$. The point group symmetry of the cation and anion sites are D_{2h} and C_{2v}. The D_{2h} symmetry of the cation site is composed of a large octahedral term plus a weaker orthorhombic distortion. The octahedral term causes the metal d levels to separate into a triply degenerate t_{2g} group, and a doubly degenerate e_g group. The orthorhombic distortion removes the degeneracy within these manifold. The C_{2v} symmetry of the anion site likewise removes the degeneracy of the oxygen $2p$ levels (Fig. 2.2).

2.2. Titanium dioxide

Titanium dioxide has been studied intensively over the last thirty years. The interest stems largely from its chemical stability, and the fact that in reduced form TiO_2 behaves as a good semiconductor, whereas pure, fully oxidised TiO_2 is an insulator with a band gap of around 3 eV. Good quality single crystals of TiO_2 grown by the flame fusion technique were available as early as 1952. Accurate band structure calculations for TiO_2 were first made in 1977 [8], and an improved calculation appeared in 1979 [9]. Good agreement exists between these theoretical models and several optical studies of TiO_2, indicating that the intrinsic properties of this material are fairly well understood. The same cannot be said for reduced and donor doped TiO_2 where much contradictory literature exists. We

will review in this section the established properties of pure oxidised titanium dioxide. Reduced and doped TiO_2 will be discussed in the next sections.

2.2.1. *Band structure calculations.* The band structure of TiO_2 has been calculated by Daude, Gout and Joanin in 1977 [8] using the tight binding approach (linear combination of atomic orbitals, LCAO) for the oxygen 2p and 2s bands, and using a pseudopotential approach for the conduction bands (Fig. 2.3). The O 2s band is found to be 4.25 eV wide and lies about 7 eV below the 2p band. The upper valence 2p band itself is found to be about 16.5 eV wide which contrasts with experimental values of around 6 eV as deduced by photoemission studies [10] and the X-ray studies of Fischer [11]. The valence band maximum is found to be a Γ_3 state at the centre of the Brillouin Zone. The next highest states are a Σ_4 state in the [110] direction, and then X_1 and X_2 states lying 0.258 and 0.394 eV below the band maximum. The lower conduction band is calculated to be 3.2 eV wide. The lowest conduction band state is a Γ_1 state and the next lowest is X_1, 0.73 eV higher.

According to this calculation TiO_2 is a direct band gap semiconductor, although the direct transition is forbidden. The optical absorption edge is supposed to correspond to the onset of indirect transitions between X and Γ extrema. The first direct allowed transitions are calculated to be at 3.45 eV for $E \perp c$, and at 3.59 eV for $E \parallel c$.

A refined calculation taking into account spin-orbit coupling was performed by Jourdan, Gout and Albert [9] for the upper valence and lower conduction bands. The calculation gives the same direct forbidden gap at Γ, and valence band maxima are found 41 meV below in the Σ [110] direction, and 75 meV below in the Δ [100] direction. The valence band width is reduced to 12.34 eV, in slightly better agreement with experiment.

2.2.2. *Optical properties.* In 1952 Cronemeyer [12] measured the optical band gap in TiO_2 at 3.03 eV, and demonstrated that it shows a strong red-shift with increasing temperature. Recently Pascual, Mathieu and Camassel [13, 14]

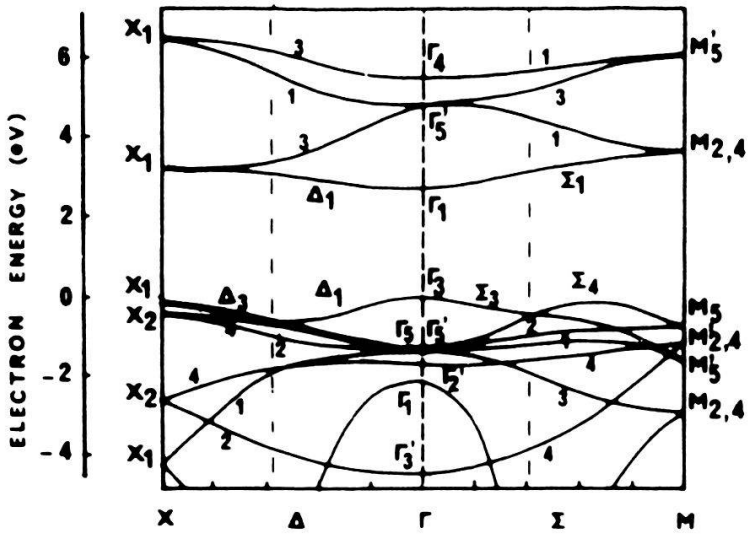

Figure 2.3
Band structure of TiO_2 near the Fermi level from Ref. 8.

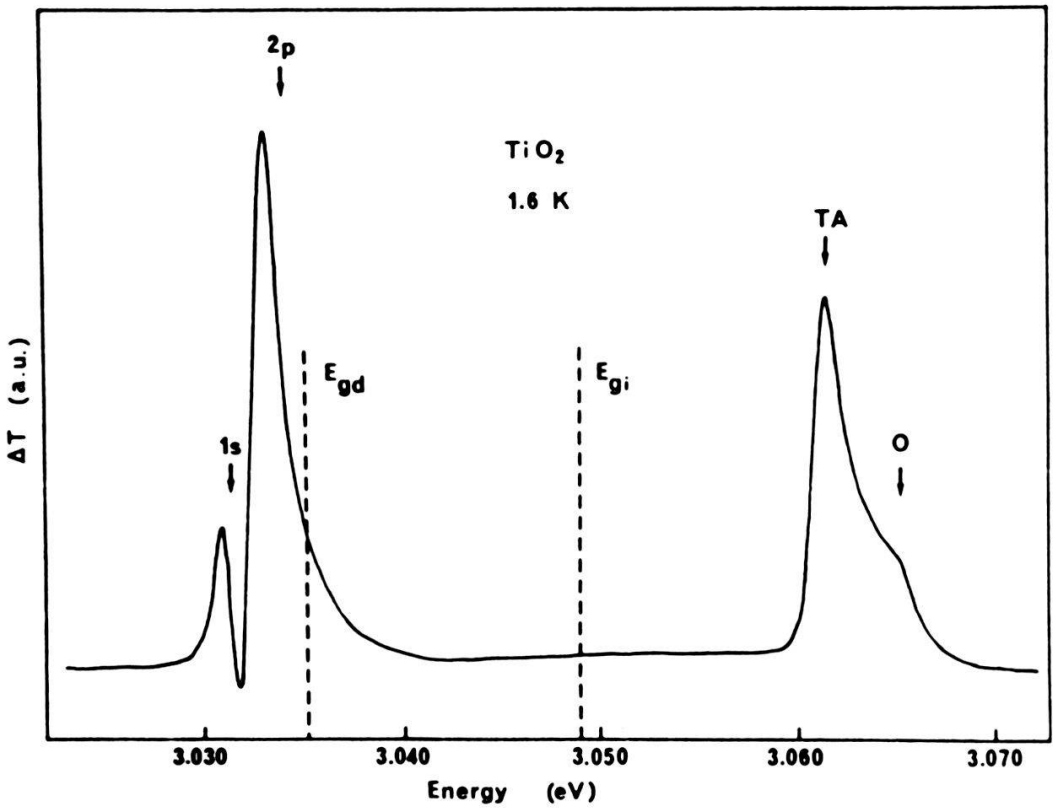

Figure 2.4
Wavelength modulated absorption spectra of TiO_2 from Ref. 14.

have resolved very fine structure in the absorption edge demonstrating the direct nature of the band gap. Using wavelength modulated absorption at 1.6 K, they identified 1s and 2p excitons associated with Daude's $\Gamma_3 \rightarrow \Gamma_1$ direct edge at 3.036 eV (Fig. 2.4). This transition is completely forbidden for $E \parallel c$ and only allowed through an electric quadrupole interaction for $E \perp c$. The indirect edge is shown to lie at 3.061 eV for both polarisations. Stress dependent measurements showed that the indirect edge arises from the valence band maximum in the Δ [110] direction near X, in agreement with both Daude and Jourdan.

Further confirmation of the band structure calculations comes from reflectivity measurements [15], electroabsorption and electroreflection [16–19] and absorption measurements on thin films [20, 21] where structure corresponding to direct, allowed transitions are observed at roughly the calculated energies. Figure 2.5 shows the absorption spectrum of a 300Å TiO_2 layer measured by Linz [20]. The indirect absorption edge at 3 eV is indistinguishable in a sample this thin, and the observed structure can be attributed to direct transitions. The absorption maximum corresponds to an absorption coefficient of about $10^6\,cm^{-1}$.

2.2.3. *Other properties.* Many X-ray and ultra-violet photoemission studies have been performed on TiO_2. While most are concerned with the density of defect and surface states in the band gap, they allow the basic valence band structures to be studied. Figure 2.6 shows a typical spectrum [22]. The valence band is found to be about 6 eV wide with two main peaks around 2.6 and 4.7 eV below the valence band edge. Unfortunately neither Daude nor Jourdan calculated the density of states from their band structure calculations, and we can only

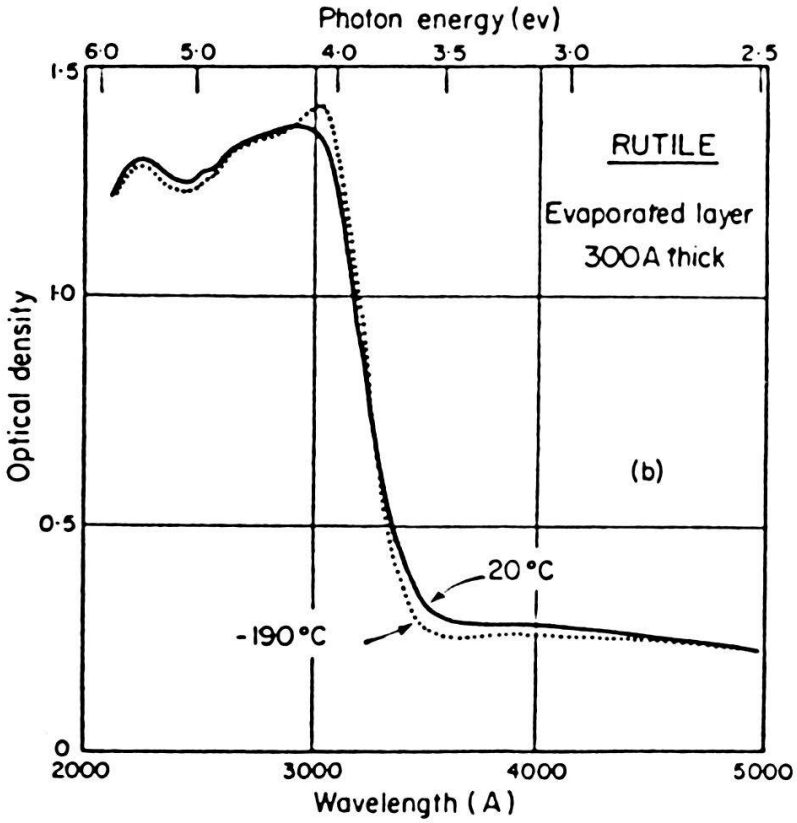

Figure 2.5
Optical density of 300 Angstrom TiO_2 film from Ref. 20, showing onset of direct allowed transitions near 3.5 eV.

note that the total valence band width in both calculations is more than twice the experimental value.

Cronemeyer [12] measured the electrical conductivity of TiO_2 at high temperature (Fig. 2.7). Up to 900°C the activation energy for conduction is 1.526 eV in both directions. This is almost exactly half the optical band gap and is strong evidence that high temperature conduction involves thermal excitation of electrons from the valence band to the conduction band. Above 900°C a higher activation energy is found. One possible explanation is of a second conduction band of higher mobility than the first lying about 0.3 eV higher. In Daude's model this could only be the Δ_3 band which descends at X to 0.54 eV above the

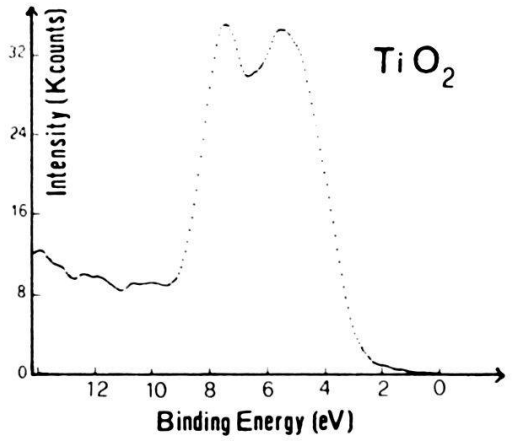

Figure 2.6
X-ray Photoemission Spectrum of TiO_2 showing valence band density of states from Ref. 22.

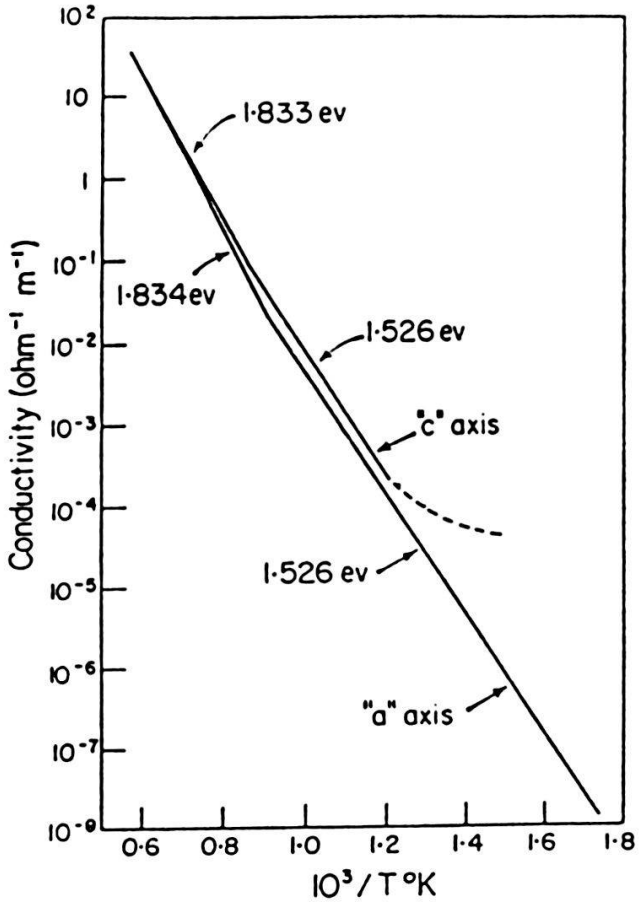

Figure 2.7
Electrical conductivity of TiO_2 at high temperature from Ref. 12.

conduction band edge. Another possible explanation is that extra carrier creation due to reversible oxygen loss occurs above 900°C as indicated by Rudolph [23]. The electronic mobility of 0.1 to 1 cm^2/V sec found in stoichiometric or lightly reduced TiO_2 is attributed to conduction in narrow bands by some authors, and to polaronic hopping by others. This is discussed further in the next section.

2.3. Reduced and donor doped titanium dioxide

It has long been known that heating TiO_2 in a reducing environment (vacuum, H_2, CO etc) transforms it from a transparent insulator into a blue-grey *n*-type semiconductor. The exact nature of the defects created, however, and the nature of the charge carriers are still controversial subjects. It is known that TiO_2 loses oxygen during reduction, and before 1962 electrical and optical measurements on reduced TiO_2 were interpreted in terms of oxygen vacancy models [20]. Later EPR experiments [24, 25] provided evidence that interstitial titanium may be the predominant defect created on reduction, but other studies [26] reinterpreted the observed signals in terms of interstitial hydrogen. A concensus seems to exist now whereby reduction at low temperatures and high oxygen pressures creates mostly oxygen vacancies, and at higher temperatures and lower oxygen pressures mostly titanium interstitials. Many recent studies [27–30] give evidence for complexes of trivalent impurity ions with titanium interstitials and oxygen vacancies. In one recent review [31], Kerssen and Volger interpret EPR signals of

reduced TiO_2 in terms of electrons trapped on interstitial Ti^{3+} ions paired with substitutional Si^{4+}, and electrons trapped by oxygen vacancies. The overall picture is therefore extremely complex and the defects formed depend not only on the reduction temperature and environment, but also on the impurities initially present in the samples.

Effects similar to reduction are produced on doping with group one elements (H, Li, Na) which occupy interstitial sites in TiO_2, and with group five elements (Nb, Ta, P) which substitute for Ti. These elements are therefore considered to be donor dopants in TiO_2.

2.3.1. *Optical and electrical properties.* The first detailed optical absorption spectra of reduced TiO_2 were published in 1959 by Cronemeyer [42]. He showed that lightly reduced titanium dioxide has a broad near infra-red absorption band with its maximum at 0.8 eV at room temperature. More strongly reduced samples show a second band at 1.18 eV. Moreover the intensity of the 0.8 eV band is proportional to the electrical conductivity. Bogomolov et al. [33] also observed the 0.8 eV peak in lightly reduced TiO_2, and showed that on cooling to 10 K, this band disappears and is replaced by a band at 1.15 eV. This change is accompanied by a strong increase in the electrical resistivity. They also showed that doping with Li or P, or reducing in H_2 produces the same 0.8 eV absorption band at room temperature. In another study [34] Bogomolov showed that Nb doped TiO_2 shows absorption bands at 0.8 and 1.2 eV at 300 K and lower temperatures, but at 600 K shows only the 0.8 eV band. Mirlin et al. [35] observed similar behaviour in partially reduced, Cr doped TiO_2. At room temperature an absorption band at 1.1 eV is present, but on heating to 800 K this weakens and is replaced by the familiar 0.8 eV band. Bogomolov found in agreement with Cronemeyer that the intensity of the 0.8 eV band at room temperature varies directly with the electrical conductivity. Heating to 900 K, however, increased the electrical conductivity but the 0.8 eV band became broader and weaker at the same time. Von Hippel showed in 1962 [20] that stochiometric titanium dioxide heated to 1300 K shows appreciable conductivity but the absorption spectrum at that temperature is featureless.

It therefore seems that the spectra of reduced or donor doped TiO_2 can be divided into three distinct domains.

i) At low temperatures the absorption spectra depend on the defect present (i.e. center created by reduction, or the dopant ion), but typically show absorption peaks in the range 1.1–1.2 eV. These spectra are associated with high electrical resistivity. The upper temperature limit depends on the type and number of defects, being 10–300 K for reduced TiO_2, around 300 K for Nb doped TiO_2, and around 600 K for reduced Cr doped TiO_2. These spectra are interpreted as being due to electrons trapped on the defect. Additional evidence for this in Nb and Ta doped, and reduced TiO_2 comes from the EPR measurements of Chester [24, 36].

ii) At intermediate temperatures the absorption spectra of reduced and donor doped TiO_2 are identical, and show a single broad peak at 0.8 eV. The intensity of this peak varies linearly with the electrical conductivity of the samples, and the peak is therefore attributed to the absorption of light by charge carriers.

iii) At high temperatures, $T > 1000$ K, the 0.8 eV band disappears and a flat, featureless absorption spectrum is found. At these temperatures even pure TiO_2 shows appreciable electronic conductivity ($\sigma > 10^{-4}\,\Omega^{-1}\,\mathrm{cm}^{-1}$).

The electrical properties of reduced and n-doped TiO_2 have been the subject of a large number of studies. In general good agreement exists between the different experimental results. Differences are found at low temperature (<60 K) between Nb doped and reduced TiO_2 which can be attributed to the greater binding energy of the Nb donors in comparison with the point defects of reduced TiO_2 [37]. This is entirely consistent with the optical studies. Above 60 K lightly doped and lightly reduced TiO_2 show essentially identical properties which can be attributed to electrons moving in the TiO_2 lattice. For typical temperature dependencies of the electrical conductivity, Hall coefficient and Hall mobility the reader is referred to Becker and Hosler [38] or other studies [39–42].

The different interpretations of optical and electrical data on TiO_2 may be divided into two distinct classes; the band models, and the small polaron models. The band models are based on the idea that conduction electrons move in a narrow Ti 3d band, with effective masses of 10–30 m_e. To explain experimental results at low temperature, some authors [43] propose a model in which the lowest conduction band, characterised by strong anisotropy ($\mu_c \gg \mu_a$) and high effective mass, overlaps with a second, nearly isotropic band, of lower effective mass. The separation of the two bands is estimated to be around 20–50 meV. Other authors [41] propose a single band model with two or more defect levels. The behaviour above 100 K is characterised by a decrease in Hall mobility with increasing temperature, attributed to carrier scattering by optical phonons. This temperature dependence of the Hall mobility is perhaps the strongest evidence in favour of the band models as opposed to hopping models. In these models the near infra-red absorption band at 0.8 eV is attributed to intraband transitions of the conduction electrons, but no explanation for the weakening of the band with increasing temperature has been offered.

Other authors argue that all available optical and electrical data on TiO_2 can be explained in terms of a small polaron model. The basic requirement is that the electron lattice coupling be strong enough to allow a conduction electron on a cation site to trap itself by inducing a polarisation of the surrounding lattice (essentially the nearest neighbour oxygen ions). In this model the experimentally measured Hall mobility is not a reliable measure of the real drift mobility. Conduction occurs via the hopping of the polaron (i.e. conduction electron plus lattice distortion) from one site to another. The observed increase in electrical conductivity with increasing temperature around room temperature, with activation energy of around 0.15 eV can be attributed to the increasing hopping mobility of the polarons. Optically stimulated transitions of the polaron require more energy than thermal transitions since the electron is excited from its well to another site faster than the lattice polarisation can follow. A simple two-node model [33] predicts that optical transitions require four times as much energy than thermal transitions, in which the lattice deformation can follow the moving electron. This gives good agreement with the activation energies deduced from electrical and optical measurements (0.15 eV and 0.8 eV). A thorough analysis shows that both the detailed form of the 0.8 eV band, and its temperature dependence can be explained in terms of the small polaron model [44]. In justifying this model however the authors show that in conduction bands less than 1 eV wide, intraband transitions could not fully account for the 0.8 eV absorption band. According to Kahn [43] a conduction band width of less than 1 eV is also a prerequisite for polaron formation. Both recent band structure calculations however [8, 9], predict considerably wider (≈3.5 eV) conduction bands.

2.4. Deep impurities in TiO_2

In addition to the donor dopants, many other impurities in TiO_2 have been studied. To understand the role played by an impurity ion in TiO_2 three questions must be answered.

i) The valence states which the ion may adopt in TiO_2.
ii) The position of the ion in the TiO_2 lattice, and the structural defects which the presence of the ion induces.
iii) The energy levels of the different valence states with respect to the TiO_2 valence and conduction bands.

The techniques used to study the impurities vary according to the ion in question. Precise information on the position of an ion in the lattice may be obtained by EPR, but only ions with magnetic moments may be studied, which excludes certain valence states (e.g. V^{4+} may be studied but neither V^{3+} nor V^{5+}). Mössbauer spectroscopy is applicable to only a few elements, but all valence states may be observed. The information that can be obtained by Mössbauer is limited however, and large doping concentrations are required. The other tech-

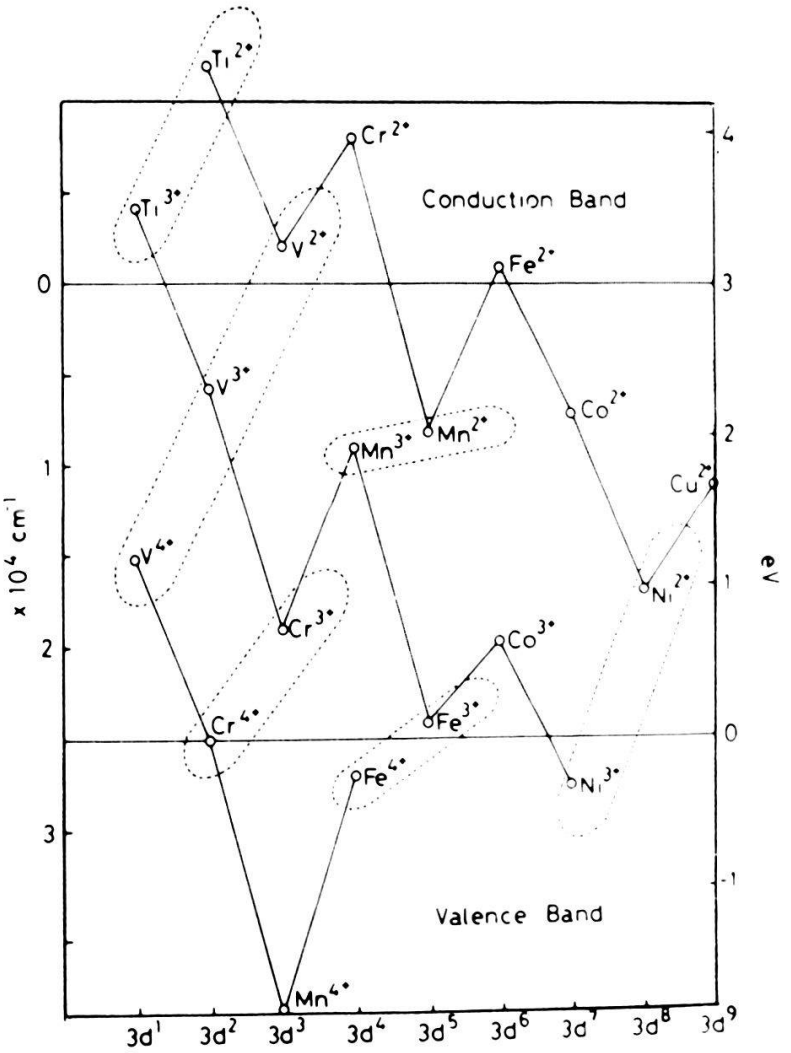

Figure 2.8
Calculated energy levels of transition metal ions in TiO_2, from Ref. 46.

niques most often used are optical absorption, electrical conductivity, photoluminescence and photoconductivity. The interpretation of these measurements usually depends on information obtained by EPR and/or Mössbauer. We will briefly review results on some deep impurities in TiO_2.

Cr

Many studies exist of Cr doped TiO_2. In 1959 Gerritsen [45] showed that Cr^{3+} substitutes for Ti^{4+} in oxidised TiO_2. Mizushima et al. [46] showed that the intensity of the Cr^{3+} EPR signal could not be altered significantly by Li doping, and deduced that the Cr^{2+} level must lie above the conduction band edge as shown in Fig. 2.8. Mirlin, Reshina and Sochava [35] deduced from optical absorption that some Cr^{4+} is present in oxidised Cr doped TiO_2, and that slight reduction converts this to Cr^{3+}. On further reduction important changes occur in the absorption spectrum which demonstrate the presence of deep defect levels created in the TiO_2 lattice by the Cr. Heating to 500°C emptied the electrons from these levels into the conduction band.

Fe

Numerous EPR studies have demonstrated that Fe^{3+} substitutes for Ti^{4+} in TiO_2. Although undisturbed Fe^{3+} ions are observed, evidence has been found [47] for Fe ions associated with various charge compensation defects including oxygen vacancies and titanium interstitials. Variations of the Fe^{3+} signal intensity on Li doping led Mizushima [46] to deduce that this ion can trap an additional electron to become Fe^{2+}, and to propose the energy levels shown in Fig. 2.8. The optical absorption spectra of Fe doped TiO_2 have been studied by Johnson et al. [48]. They observed enhancement of the intrinsic absorption edge when TiO_2 was doped with both H and Fe. This absorption can probably be assigned to excitation of electrons from Fe^{2+} to the conduction band. A slight enhancement of the edge observed by Wittke [49] in Fe doped, oxidised TiO_2 may be due to valence band to Fe^{3+} transitions. Interpretation of the spectra is complicated by the tendency of Fe to form precipitates in TiO_2. A study of ion implanted Fe in TiO_2 using ^{57}Fe Mössbauer spectroscopy [50] showed both Fe^{2+} and Fe^{3+} but clear evidence of iron rich phases was found.

Al

EPR studies have shown that Al doping produces complex defects in TiO_2. Substitutional Al^{3+} has been shown [51] to trap holes on the nearest neighbour oxygen ions. Pairing of Al^{3+} ions in the *c*-direction was also observed. Pairing of substitutional and interstitial Al^{3+} (self compensation) was deduced from EPR by Kerssen and Volger [31]. This centre can trap two electrons which are located on neighbouring Ti ions.

Ga

Zwingel [52] showed that substitutional Ga^{3+} can trap holes on neighbouring oxygen ions. The formation of Ga_4TiO_8 complexes in TiO_2 has been observed, even at low Ga concentrations [53].

Mizushima also studied EPR signals of Mn and V in TiO_2 and their intensity variations with Li doping, giving the energy levels shown in Fig. 2.8. We conclude that many elements have two or more stable valence states in TiO_2 enabling them to trap electrons introduced by donor doping or reduction. Ions in a valence state of three or less are often associated with charge compensation defects (oxygen vacancies or interstitial metal ions), or provoke precipitation of impurity rich phases from the lattice. In some cases however, charge compensation occurs over relatively long distances, as shown by EPR of Fe^{3+}.

The group three elements Al and Ga have been shown to induce holes in the neighbouring oxygen ions. Some evidence that undoped TiO_2 shows weak *p*-type conduction has been given [20], probably due to the presence of some trivalent impurities. Appreciable *p*-type conductivity cannot be induced however, because of the ease of charge compensation defect formation.

2.5. Ruthenium dioxide

The majority of studies on RuO_2 concern its unique electrochemical properties as an oxygen or chlorine evolution anode. A number of studies exist however of its fundamental physical properties, and together with the band structure calculation of Mattheiss [5] they give a coherent picture of this material.

In the calculation of Mattheiss the oxygen 2p band has a width of about 5 eV. The 2s band is narrower, and lies 11 eV below the 2p band. Overlap and covalent mixing with the oxygen 2s and 2p bands splits the ruthenium 4d band into a higher e_g and a lower t_{2g} part. The total 4d band width is about 6 eV. Covalent mixing with the oxygen bands raises the energy of the ruthenium 5s and 5p bands well above that of the 4d band.

From the band structure, Mattheiss calculated the density of states curve for RuO_2 (Fig. 2.9). The labels p_{1-4}, d_{1-4} etc are those of Goel et al. [54]. The ligand field splitting of the 4d bands is clear, and the separation of the Ru 4d bands from the oxygen 2p bands is found to be 2.3 eV. A feature of this type of calculation, however, is the overestimation of the p–d energy separation by several eV.

The valence band density of states of RuO_2 has been studied by X-ray photoelectron spectroscopy (XPS) by Riga et al. [22]. The agreement between the experimental and calculated positions for the density of states maxima of the oxygen 2s and 2p bands, as well as for the ruthenium peak d_1 is very close.

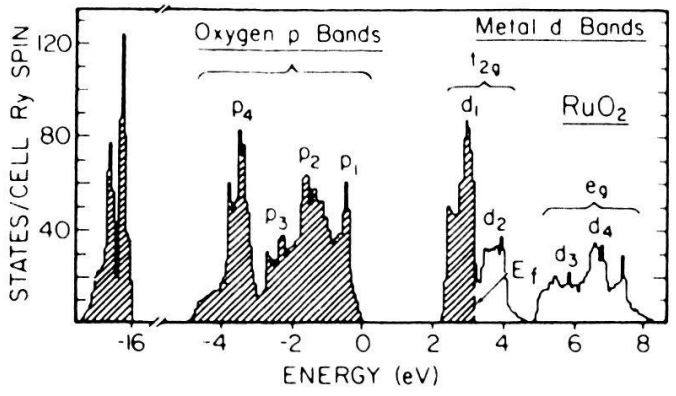

Figure 2.9
Electronic density of states in RuO_2 from Ref. 5.

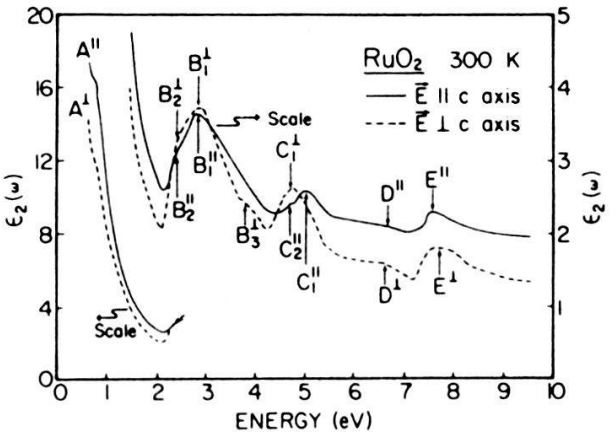

Figure 2.10
Imaginary part of the Dielectric Constant ϵ_2 of RuO_2 from Ref. 54.

The Fermi surface, and the structure of the 4d t_{2g} bands have been studied through magnetothermal oscillations by Graeber et al. [55]. Both were in close agreement with the calculation of Mattheiss. The Fermi surface has also been probed by observation of the De Haas–Van Alphen effect [56]. Three characteristic frequencies were found, corresponding to effective masses of $0.51m_e$, $1.7m_e$ and $3.5m_e$, where m_e is the mass of a free electron.

The optical reflectivity of RuO_2 has been studied by Goel et al. [54]. The spectrum shows the plasma edge near 2 eV, and a series of reflectivity maxima corresponding to interband transitions. The imaginary part of the dielectric constant is shown in Fig. 2.10. The structures A to E are interpreted in terms of the electronic density distribution peaks shown in Fig. 2.9, as follows:

A ($h\nu < 2.0$ eV) Free carrier and d electron intraband transitions.
B ($h\nu \approx 2.8$ eV) O $2p_1$ to Ru $4d_2$ transitions.
C ($h\nu \approx 5.0$ eV) O $2p_3$ to Ru $4d_2$ transitions.
E ($h\nu \approx 7.5$ eV) O $2p_2$ to Ru $4d_4$ transitions.

The above interpretations require that the p–d band gap in the calculation of Mattheiss be reduced by about 1 eV. This is a reasonble adjustment in view of the known tendency of LCAO calculations to exaggerate band separations, but goes against the XPS evidence of Riga.

Various authors have studied the electrical transport properties of RuO_2. The most complete investigation is that of Ryden, Lawson and Sartain [57]. They have shown that the electrical resistivity of RuO_2 can be accurately described by an equation of the type:

$$\rho(T) = \rho_0 + \rho_2 T^2 + \rho_3 T^3 [J_3(\theta_D/T) - J_3(\theta_E/T)] \quad (1)$$

where ρ_0 is the resistivity at zero Kelvin, J_3 is a standard transport integral, θ_D is the Debye temperature, and θ_E is a parameter characterising the momentum gap between low and high mobility bands. ρ_2 and ρ_3 represent the magnitudes of the T^2 and T^3 terms. The T^2 and T^3 terms originate from electron – electron and electron – phonon interband scattering, although other scattering mechanisms may have the same temperature dependencies. The success of an interband scattering model in fitting the resistivity data implies that the Fermi surface consists of bands with widely varying electronic mobilities. This is entirely consistent with the De Haas–Van Alphen measurements of Marcus and Butler showing sevenfold mobility variations in the different Fermi surface layers.

The optical and electronic properties of RuO_2 will be further discussed in Chapter four.

2.6. TiO_2–RuO_2 mixed systems

Until now mixed TiO_2–RuO_2 samples have been prepared by one of two methods. The simplest technique is to mix intimately TiO_2 powder with Ru or $RuCl_3$. Sintering then oxidises the ruthenium to RuO_2 which may interdiffuse with the TiO_2. This produces so called "ceramic" samples. The other technique is to prepare a solution of the chlorides $TiCl_4$ and hydrated $RuCl_3$ in a suitable solvent (e.g. isopropanol) and to apply this (often with a brush) to a substrate, usually titanium. This is then heated in air or oxygen to eliminate the solvent and to convert the chlorides to the dioxides (pyrolysis). This technique is close to that used commercially to prepare electrodes. The properties of layers prepared in this way depend strongly on the pyrolysis temperature. Low temperature ($T < 700°C$) treatments produce single phase layers throughout the TiO_2–RuO_2 composition range, while high temperature treatments ($T \geqslant 700°C$) produce two phases, one close to TiO_2 in composition, and the other close to RuO_2.

2.6.1. *Thin film $Ti_{1-x}Ru_x$ solid solutions.* The microstructure of the $Ti_{1-x}Ru_xO_2$ layers prepared by low temperature pyrolysis was studied by Lebedev et al. in 1976 [58]. Films treated at 450°C showed a single rutile structure phase throughout the composition range, although on the TiO_2 rich side an anatase phase was also present. The lattice parameters of the rutile phase were found to vary monotonically with the composition. The degree of crystallinity was found to be low, however, and the layers contained several atomic percent of chlorine. It was found that preparation of bulk rather than thin film samples, using the same technique produced two rutile phases with only weak intersolution. Galyamov [59] measured the optical and electrical properties of the thin film $Ti_{1-x}Ru_xO_2$ solid solutions. The composition dependence of the electrical conductivity was found to be:

$$\sigma_x/\sigma_1 = (x - x_c)^{1.6} \quad (x_c \leqslant x \leqslant 1)$$

where σ_1 is the conductivity of RuO_2 films, and x_c is the composition of the conduction threshold, found to be 0.25. This relation is consistent with conduction along infinite RuO_2 clusters. Optical absorption measurements in the infra-red also indicated the presence of these clusters. The conductivity of pure RuO_2 films was about three orders of magnitude lower than that of RuO_2 single crystals at room temperature, and increased with temperature in some temperature ranges. This indicated activated conduction, and the sign of the thermoelectric power was positive, indicating *p*-type conduction. The authors deduced that the disorder in the films resulted in a deep pseudogap at the Fermi-level.

The optical and electrical properties of the $Ti_{1-x}Ru_xO_2$ solid solutions were further studied by Roginskaya et al. [60] in the insulating TiO_2 rich domain ($x < 0.25$). The diffuse reflectivity of samples in the region of the fundamental TiO_2 edge was measured. It was found that in samples containing ruthenium, absorption occurred at sub-band gap energies. The authors attribute this to smearing of the valence and conduction band edges by disorder.

X-ray photoelectron spectra of the titanium core levels indicated partial

electron transfer from the RuO_2 clusters to the TiO_2 matrix. The transfered electrons are not localised on Ti^{3+} ions, but appear to be free in the Ti 3d conduction band. This metallic behaviour of TiO_2 is limited however to the immediate vicinity of the RuO_2 clusters where its conduction band is modulated by strong random electric fields. The solid solution in these films has been shown to be metastable, and decomposes to a chlorine free two phase TiO_2–RuO_2 system on heating at 700–800°C [61, 62].

2.6.2. *Two phased TiO_2–RuO_2 systems.* $TiCl_4$–$RuCl_3$ films pyrolysed at 700°C or above are similar to the ceramic samples. In both cases two phases are present, one close in composition to RuO_2, and the other close to TiO_2. Lebedev et al. [58] found that the solubility of TiO_2 in RuO_2 in ceramic samples is 8–9 mol%. Galyamov et al. [63] investigated the electrical conductivity and thermoelectric power of Ti doped RuO_2 samples prepared in this way. Pure RuO_2 samples were shown to be metallic. The presence of Ti was shown to increase the resistivity and this is attributed to a reduction in the mean free path of the conduction electrons. Activated conduction appears above 700°C when 4% TiO_2 is present, and this is attributed to formation of a pseudogap at the Fermi-level. Doping with 10% TiO_2 increases slightly the resistivity, and a TiO_2 rich phase appears. The temperature of the transition from metallic to activated conduction is unchanged indicating that this is a property of the solid solution, rather than due to the bulk TiO_2. Effects due to the grain boundaries present in all ceramic samples were not considered.

The properties of the Ru doped TiO_2 phase were studied by Roginskaya et al. [64]. The solubility of Ru in TiO_2 increases with temperature, and is about 6% at 1350°C. The variation of electrical conductivity with the partial oxygen pressure was studied for samples with 1.1 and 2.6% Ru. The measurements were performed at 1000°C and above. It is known that reduction of TiO_2 creates donors, and the variation of the conductivity with reduction therefore indicates if the carriers initially present were electrons or holes. The variations observed indicated n-type conduction. The dependence of σ on P_{O_2} in one sample was typical of an oxide with triply charged impurities. Since this was the more strongly doped sample Roginskaya proposed that some ruthenium was present as Ru^{3+}. The variation of the Seeback coefficient with Ru concentration also indicated that Ru could behave as an acceptor, and that conductivity at low temperatures is mixed n and p-type. On the basis of these results. Roginskaya proposed that both Ru^{4+} and Ru^{3+} can substitute for Ti^{4+} in TiO_2.

Thermogravimetric measurements on Ru doped TiO_2 ceramic samples were performed by Valigi and Gazzoli [65]. A sample doped with 5% Ru, of which 1.8% was in solid solution was heated in hydrogen. Three sharp weight loss steps were observed. The first at around 180°C is attributed to reduction of the bulk RuO_2 to Ru metal. The other two steps were of equal intensity and resulted in the reduction of the dissolved Ru to Ru metal. They were interpreted as:

i) Ru^{4+} to Ru^{2+}, occurring between 350 and 525°C.
ii) Ru^{2+} to Ru metal, involving precipitation from the lattice, and occurring between 525 and 750°C.

Reduction of TiO_2 occurred only above 750°C. From these measurements Valigi proposed that Ru^{4+} and Ru^{2+} could substitute for Ti^{4+} in TiO_2.

3. Crystal growth

Until now TiO_2 and RuO_2 have always been grown by different techniques; closed system chemical vapour transport (CVT) for TiO_2 using halide transport agents, and open system CVT for RuO_2 in flowing oxygen. To produce crystals in the TiO_2–RuO_2 system it is necessary to use a growth technique suitable for both oxides. We found that the traditional closed system CVT using halides could also be used for RuO_2, and even enabled the growth of better pure RuO_2 crystals at 1000°C than could be grown in open system at the same temperature.

The chemical vapour transport (CVT) of TiO_2 by halide transport agents has already been described by Schäfer [66] using HCl, Izumi [67] using NH_4Cl and NH_4Br, and by Dartyvan [68] and Niemyski [69] using $TeCl_4$. We have found that RuO_2 may be transported by a number of halides. Best results for pure RuO_2 were obtained using HCl, and for Ru doped TiO_2, using $TeCl_4$. The reactions involved in transport are typified by the transport of TiO_2 using $TeCl_4$. The overall reaction may be considered to be:

$$TiO_2(s) + TeCl_4(g) \rightarrow TiCl_4(g) + TeO_2(g) \quad (1)$$

There is a large entropy increase (220 J. mol^{-1}. K^{-1}) in the sense left to right, and therefore the equilibrium constant moves to the right with increasing temperature. If an ampoule containing TiO_2 and $TeCl_4$ is placed in a temperature gradient, the overall effect of the reactions in equation (1) is the transfer of TiO_2 to the coldest end of the ampoule, where single crystals may be obtained. In fact $TeCl_4$ dissociates according to the reaction:

$$TeCl_4(g) \rightarrow TeCl_2(g) + Cl_2(g)$$

This can lead to rapid temperature oscillations and turbulent gas flow during growth experiments, as well as to strong deviations of the temperature inside the ampoule from that outside. Rosenberger [70] discussed these problems in detail, and reported that they lead to irregular crystal growth. Care must therefore be taken in choosing growth parameters which diminish the risk of turbulence, and for this reason we chose to use horizontal growth ampoules, to work at temperatures where disassociation is complete, and to use moderate temperature gradients. For all our growth experiments we have used 12 cm long quartz ampoules of internal diameter 15 mm. These are placed in a tubular two zone furnace of internal diameter 65 mm. For all crystals in the TiO_2–RuO_2 system, a source temperature of 1050°C, and growth temperature of 1000°C gives good results. For samples containing tantalum, gradients of just 20° are used, since stronger gradients lead to inhomogeneous tantalum distribution within the crystals.

We have attempted growth of pure and doped TiO_2 and RuO_2 using a number of transport agents. Fastest growth (~1 g per week under the conditions given above), and the best quality doped TiO_2 crystals were obtained using 300 mg of $TeCl_4$. For RuO_2, transport with $TeCl_4$ is rapid but gives poor quality crystals, and HCl is preferred, although transport is slower (~0.3 g per week).

Figure 3.1 shows some RuO_2 crystals grown using HCl as the transport agent. These are comparable in size with those of Huang [71] but are obtained at much lower temperature. The TiO_2 crystals doped with Ru, Ta and Nb grown with $TeCl_4$ are similar in size to the RuO_2 crystals shown.

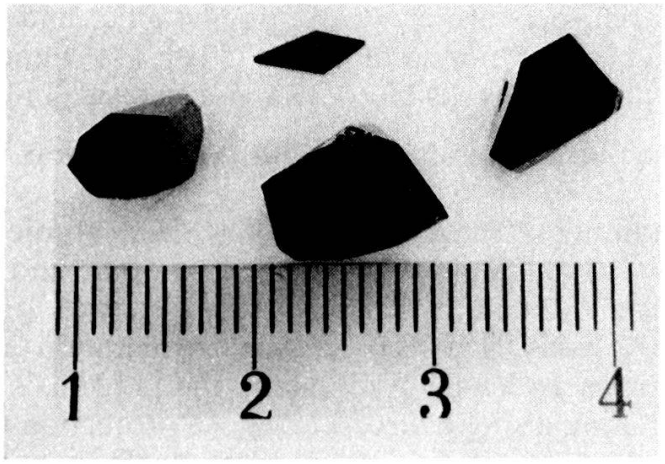

Figure 3.1
RuO_2 single crystals grown in closed ampoules using HCl.

The crystals of the $Ti_{1-x}Ru_xO_2$ family can be separated into three groups, with distinct physical properties, according to their composition.

(i) The TiO_2 rich crystals, $x \leqslant 0.02$, are insulating ($\rho > 10^9\ \Omega$ cm) at room temperature. They vary in colour from transparent for pure TiO_2 to deep red for 2 mol% RuO_2. They grow with (111), (110) and (100) faces.
(ii) Crystals with $0.02 < x < 0.98$ are matt grey and contain two phases, but have crystallographically identifiable faces and edges. Their electrical resistivity decreases from around $10^4\ \Omega$ cm for $x = 0.03$, to metallic for $x = 0.45$.

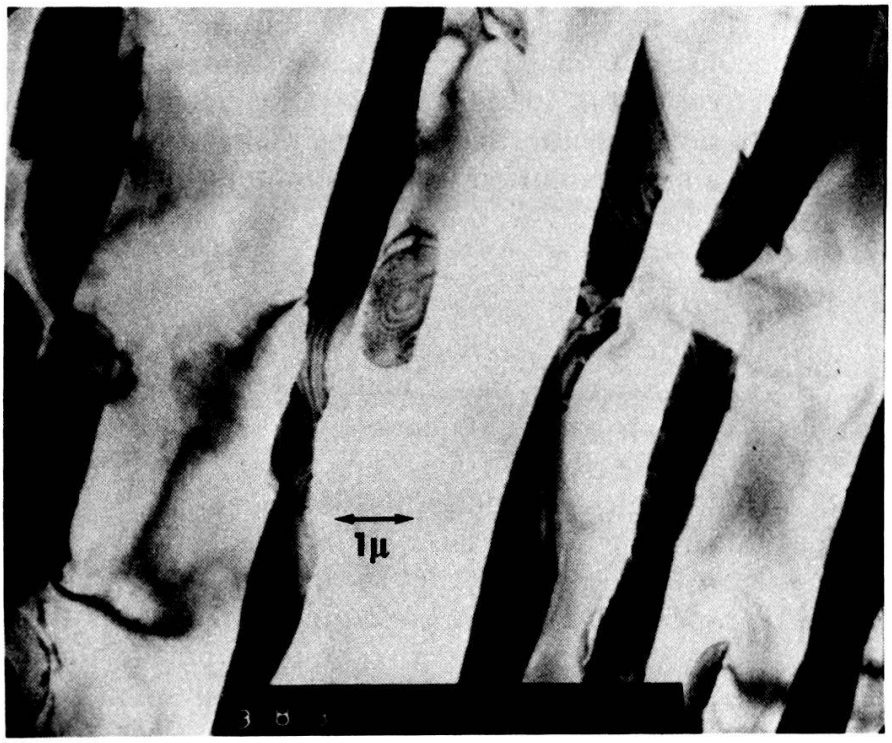

Figure 3.2
Transmission Electron Microscope image of RuO_2 rich plates in two phased $Ti_{0.9}Ru_{0.1}O_2$ crystal.

(iii) The RuO_2 rich crystals, $x \geq 0.98$ are metallic, and deep blue-black in colour. The best developed faces are (110), (111) and (100) as for TiO_2, with small (101) faces visible between adjacent (111)s.

The variation of the lattice parameters with concentration has been discussed previously [72].

A sample containing 10 mol% RuO_2 has been studied by Transmission Electron Microscopy. The sample was polished to 50 μ, and thinned further by argon ion etching. The ruthenium rich phase is present as long thin plates, lying on or close to (111) planes, and has the same orientation as the titanium rich matrix. Figure 3.2 shows an image taken along the $[11\bar{3}]$ axis of the sample. The plates are elongated along a single direction whose projection in this plane is close to [245]. The fact that the plates are elongated along only one of the four equivalent ⟨245⟩ directions demonstrates that they form during crystal growth, rather than by precipitation after growth.

4. Study of RuO_2 containing Ti

We have studied pure RuO_2 and RuO_2 containing 2 mol% TiO_2 by optical reflectivity and electrical resistivity. Both techniques have already been applied to pure RuO_2, as discussed in Chapter 2. Our aim is to investigate the modifications in the properties of RuO_2 induced by the presence of Ti in solid solution.

The optical spectra of RuO_2 show structure related to electronic interband transitions, as well as intraband and free election effects. This allows us in principle to deduce whether the Ti provokes changes in the free electron density, or in the band structure near the Fermi-level.

Electrical resistivity measurements on metals provide essentially information on the carrier scattering mechanisms. The contribution to the resistivity from different scattering mechanisms may have the same temperature dependence, and it is therefore difficult to establish unambiguously which mechanisms are dominant. The contribution from defect scattering is independent of temperature however, and is the most important contribution at very low temperatures ($T < 10$ K).

4.1. Optical reflectivity

The near-normal incidence reflectivity of pure RuO_2 has been studied in the range 0.5–9.5 eV by Goel, Skorinko and Pollak [54]. The imaginary part ϵ_2 of the dielectric constant shows structure which can be attributed to free electron absorption and intra- and interband transitions. Good agreement is found with the theoretical density of states calculated by Mattheiss [5].

We have measured the near-normal incidence reflectivity of a single crystal RuO_2 (111) face, and an RuO_2: 2% TiO_2 (110) face. Both crystals were grown by Chemical Vapour Transport (CVT) in closed ampoules [72]. As the natural faces were slightly uneven they were polished using alumina powder in stages down to 0.05 μ, and were rinsed in distilled water before measurement.

The reflectivity was measured in the ranges 15,000–2500 nm using a Beckman 4240 spectrometer, and 2500–230 nm using a Beckman Acta M VII spectrometer. The spectra obtained are shown in Fig. 4.1. The pure RuO_2 crystal has

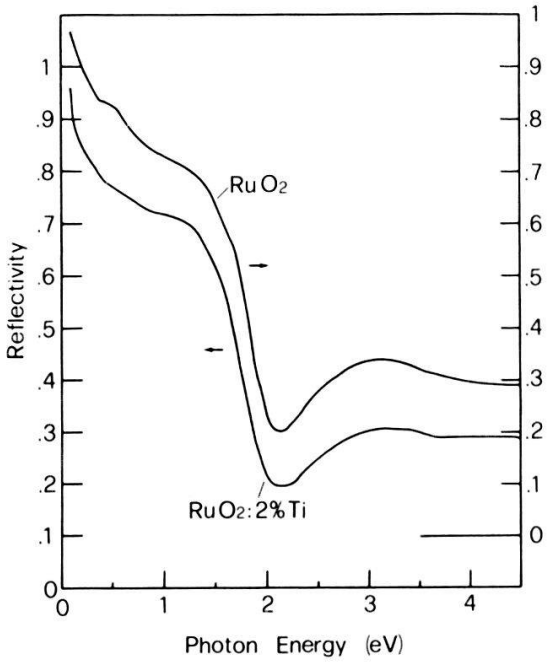

Figure 4.1
Reflectivity at 300 K of a RuO_2 (111) face, and a RuO_2–2% TiO_2 (110) face.

a higher reflectivity below 1.2 eV where free electron and intraband transitions contribute. The true position of the plasma edge is masked by the onset of interband transitions, but as far as can be seen no significant difference in position exists between the pure and doped samples. We estimate the plasma edge to be near 2.2 eV in both cases. From the electron effective mass extrema measured by Marcus and Butler [56] we estimate that the free electron mass is a good approximation for the effective mass m in RuO_2, in the equation [73]:

$$\omega_p^2 = ne^2/\epsilon_0 m$$

where ω_p is 2π times the plasma frequency, e is the charge of the electron and ϵ_0 is the free space permittivity. This gives a density of carriers, n of 4 $10^{21}/cm^3$, approximately one tenth of an electron per ruthenium ion. The first maximum due to interband transitions is at 3.1 eV, and is stronger in the pure sample. We did not observe the peak at 5.0 eV reported by Goel.

Before interpreting these measurements we should note that the reflectivity of RuO_2 is anisotropic [54]. In particuliar the perpendicular component (i.e. $E \perp c$) is stronger than the parallel component ($E \parallel c$) below 1 eV, and the reflectivity peaks due to interband transitions are all stronger in the $E \perp c$ spectrum than in the $E \parallel c$ spectrum. Our measurements were made using unpolarised light. In the case of the RuO_2 sample measured, a (111) face was used, which contains the lattice vectors [110] and [112]. Taking into account the lattice parameters, our measurement is a mixture of the parallel and perpendicular components respectively in the proportions 22% : 78%. The doped sample was measured on a (110) face which means that the mixture is 50% : 50%. We see that the pure sample spectrum contains a higher proportion of the perpendicular component. This fact alone accounts for the observed differences between the two samples.

In conclusion our optical spectra of both pure and Ti doped RuO_2 show the free electron and intraband structures observed by Goel. We also observe the peak et 3 eV attributed to the first p–d interband transitions. No significant

differences were found between the spectra of pure and doped samples, apart from those which can be attributed to the intrinsic anisotropy of RuO_2.

4.2. Electrical resistivity

In 1965 Colquitt [74] showed that the electrical resistivities of many transition metals can be accounted for by a model involving the scattering of conduction electrons from a high mobility band to another of higher effective mass and lower mobility. The conduction electrons are scattered by phonons, by defects, and by other electrons. The contribution to the resistivity from electron–phonon scattering varies as T^3 for interband scattering and as T^5 for intraband scattering. The electron–electron contribution varies as T^2.

Ryden et al. [57] applied the model of Colquitt to RuO_2, and showed that the experimental data on single crystals could be fitted by an equation of the form:

$$\rho(T) = \rho_0 + \rho_2 T^2 + \rho_3 T^3 [J_3(\theta_D/T) - J_3(\theta_E/T)] \tag{4.1}$$

where T is the absolute temperature, θ_D is the Debye temperature, θ_E is a parameter characterising the momentum gap between high and low mobility bands, and J_3 is a standard transport integral which has been tabulated [74]. ρ_0, ρ_2 and ρ_3 are the magnitudes of the T^0, T^2 and T^3 terms respectively.

The resistivity at 0 K is ρ_0. ρ_2 can be chosen to fit the resistivity variation in the range 10–20 K. θ_D is estimated from the temperature dependence of the resistivity in the range 100–300 K, θ_E from the dependence in the range 40–100 K, and ρ_3 is used to normalise the equation to the experimental value at 300 K. The Debye temperature deduced by Ryden et al. from their resistivity data is 900 ± 50 K.

The residual resistivity ratio (RRR) defined as $R_{300\,K}/R_{4.2\,K}$ is often taken as a measure of sample quality. Published values for RuO_2 vary from 20 to 800 [57].

We have measured the resistivity of pure RuO_2 grown by both open [75] and closed system CVT and RuO_2 containing 2% TiO_2 grown by closed system CVT [72]. The samples were taken as grown or polished to an oblong shape leaving at least one natural face. Spots 0.1 mm in diameter of gold on chromium were evaporated onto the natural face, and gold wires were soldered onto them. All measurements were performed using the four point method to eliminate the resistances of connecting wires and contacts. A.c. measurements at 1357 Hz with a Lock-in amplifier were preferred to d.c. techniques as they gave a better signal to noise ratio and enabled lower currents to be used, thereby reducing heating effects in the samples.

The sample geometry did not allow the absolute values of the resistances to be deduced. The resistivity of pure RuO_2 is well established however and published values only vary from $2\times10^{-5}\,\Omega$ cm [71] to $5\times10^{-5}\,\Omega$ cm [76, 77]. According to Ryden the resistivity is isotropic within experimental error at all temperatures below 1000 K.

Figure 4.2 shows the resistivities of pure RuO_2 and RuO_2:2% Ti normalised to one at 300 K. The continuous lines are theoretical curves using equation (4.1). The data for pure RuO_2 is from a measurement on a crystal grown by open system CVT, but is typical of all RuO_2 samples examined. The values of Ryden for the variables ρ_0, ρ_2, ρ_3, θ_D and θ_E (Table 4.1) gave a reasonable fit to our data, but an improvement above 70 K was obtained by using $\theta_D = 970$ K, and in

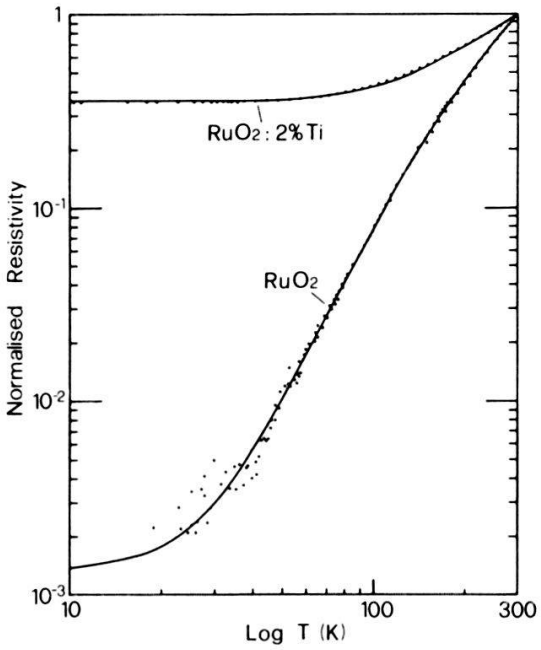

Figure 4.2
Temperature dependence of the resistivity of pure RuO_2, and RuO_2 containing 2% TiO_2.

the range 40–80 K using $\theta_E = 120$ K. To fit our data below 30 K we introduced a defect scattering value ρ_0 of 4×10^{-8} Ω cm. The RRR of this sample is 790 which is a fairly good value for RuO_2.

Having only relative values for the resistance means that only the relative magnitudes of ρ_0, ρ_2 and ρ_3 can be deduced. It is improbable however that ρ_2 or ρ_3, vary strongly from one RuO_2 sample to another, whereas ρ_0 is very sensitive to the concentration of defects or impurities present. The difference between the pure and doped samples is very clear in Fig. 4.2, and the RRR of the doped sample is only 2.8. This data has also been fitted using equation 4.1. Again a reasonable fit was obtained using the values of Ryden for ρ_2, ρ_3, θ_D and θ_E, and using $\rho_0 = 1.6 \times 10^{-5}$ Ω cm. A slightly better fit is obtained using 800 K for θ_D and 1.35×10^{-5} for ρ_0. The values used for ρ_2, and θ_E have a negligible influence on the curve, as the low temperature resistivity is completely dominated by the defect term ρ_0. The temperature dependence above 30 K demonstrates that the sample retains its metallic nature, and at room temperature the sample did not "appear" any more resistive than pure RuO_2 samples. This is reasonable since at 300 K the defect contribution is only a third of the total resistivity.

Table 4.1
Parameters of equation 4.1 giving best fit to Resistivity Data, and RRR found.

	ρ_0(Ω cm)	ρ_2(Ω cm/K^2)	ρ_3(Ω cm/K^3)	θ_D	θ_E	RRR
RuO_2 [57]	0	$3.5\ 10^{-11}$	$3.2\ 10^{-13}$	900	90	≤800
RuO_2	$4\ 10^{-8}$	$3.5\ 10^{-11}$	$3.2\ 10^{-13}$	970	120	790
RuO_2:Ti	$1.3\ 10^{-5}$	$3.5\ 10^{-11}$	$3.2\ 10^{-13}$	800	90	2.8

4.3. Discussion

Galyamov et al. [63] deduced from resistivity measurements on mixed TiO_2–RuO_2 ceramics that the presence of a few percent of Ti in RuO_2 produces a

sharp reduction in the density of states at the Fermi-level, which leads to activated conduction above 700°C. It must be noted however that measurements on ceramic samples are notorious for being inconsistent with true bulk properties as measured on single crystals. This has been shown for IrO_2 by Ryden et al., for CrO_2 by Rodbell et al. [78] and also for ReO_2 from comparison of the results of Rogers [79] and Gilbart [80].

Since TiO_2 has the same crystal structure as RuO_2, we expect the Ti ions in solid solution in RuO_2 to replace the Ru ions substitutionally. The presence of Ti on a Ru site will provoke local lattice strain, since the ideal metal–oxygen bond lengths are different (Table 2.2). The breakdown of periodicity associated with the strain field and impurity ion may have some effect on the band structure of the crystal. From our data we infer that this effect is small, but that the lattice strain field is a scattering centre for conduction electrons. In particular we deduce that the formation of a pseudogap as proposed by Galyamov does not occur on doping with up to 2% Ti, since this would have a marked effect on the number of carriers, and hence on the position of the plasma edge.

5. Study of Ru doped TiO_2

We present in this section a study by several experimental techniques of the role played by ruthenium in titanium dioxide, and we attempt to answer the three questions:

i) The valence states of ruthenium which are stable in TiO_2.
ii) the position adopted by ruthenium in the rutile lattice.
iii) The energy levels of the different valence states with respect to the valence and conduction bands of titanium dioxide.

An answer to the first two questions is provided by Mössbauer spectroscopy [5.1] and electron paramagnetic resonance [5.2]. In the light of these results we have analysed the optical [5.3] and electrical [5.4] properties of ruthenium doped titanium dioxide, and established the energies of the different valence states observed. In order to vary the Fermi level of the system, and therefore the ruthenium valence state we have used the method of donor doping as used by Mizushima [46]. In this case we dope substitutionally with Ta instead of diffusing interstitial Li into already grown crystals, as this gives a better control of the donor concentration. In the optical study we have also used reduction in hydrogen and in vacuum to vary the Fermi-level, and differences are found between the effect of these treatments, and that of donor doping.

In Section 5.5 we present a photoelectron study characterising the TiO_2:Ru surface. The results are reviewed and discussed in Section 5.6 where an energy level diagram for ruthenium in TiO_2 is proposed.

5.1. Mössbauer spectroscopy

The Mössbauer absorption of the 89.4 keV γ-rays of ^{99}Ru has been widely used in solid state applications in recent years. The Mössbauer transition takes

place between an excited state with spin and parity $\frac{3}{2}^+$, and the $\frac{5}{2}^+$ ground state. The difference in energy between the two states depends on the electronic charge density at the nucleus. This charge arises almost entirely from s electrons, with a weak $p_{1/2}$ contribution. The valence d electrons have a zero charge density at the nucleus, but influence the total density by screening the s states. The energy of the Mössbauer absorption depends therefore on the number of d electrons present. The difference in energy between the absorption in a sample, and in metallic ruthenium is called the isomer shift, and can be used to deduce the valence state of the ruthenium in the sample.

In the presence of an electric field gradient (EFG) at the nucleus, the excited state splits into a spin $\frac{3}{2}$, spin $\frac{1}{2}$ doublet, and the ground state into a spin $\frac{5}{2}$, $\frac{3}{2}$, $\frac{1}{2}$ triplet. The absorption spectrum therefore contains six lines corresponding to the six possible transitions between ground and excited states. Except in the presence of an exceptionally strong EFG, the triplet splitting is too small to be resolved, and the spectrum consists of a single line, or of two lines whose separation corresponds to the quadrupole splitting of the excited state, with structure due to the ground state splitting. A clear introduction to these effects in ^{99}Ru Mössbauer spectroscopy is given by Gütlich [81].

From an analysis of the spectra of polycrystalline samples it is possible to deduce the ruthenium valence state in the sample, the strength, and in favourable cases the sign, of the EFG. In single crystal spectra the intensity of each of the six lines varies according to the direction of the γ radiation with respect to the EFG tensor. It is therefore possible to deduce the sign and orientation of the EFG at the ruthenium nucleus. A complete analysis has been possible however, only for a small fraction of the compounds studied by ^{99}Ru Mössbauer spectroscopy [82].

In this study we have measured the ^{99}Ru 89.4 keV Mössbauer absorption in samples of ruthenium doped titanium dioxide, in titanium dioxide doped with both ruthenium and tantalum, and in ruthenium dioxide. The valence state of ruthenium in TiO_2, and the changes in valence state on addition of tantalum have been established, and the EFG strength, sign and direction have been deduced for ruthenium both in RuO_2 and TiO_2.

Experimental

All samples used in this study were single crystals prepared by chemical vapour transport. The Ru doped TiO_2 (rutile) samples contained 2% of enriched ^{99}Ru. A single crystal with large (100) faces was used for the measurements with $\gamma \parallel [100]$, and for the $\gamma \parallel [001]$ measurements many single crystals were cut into (001) slices and these were assembled to form a plate of $10 \times 10 \times 2$ mm, with the [001] direction perpendicular to the plate. A large single crystal of TiO_2: 1% ^{99}Ru + 0.3% Ta was studied with the γ-ray direction parallel to [100] and [001]. A polycrystalline sample with average doping levels of 1% Ru and 1.5% Ta was also studied. Finally (001) and (110) plates cut from a single RuO_2 crystal, and a polycrystalline RuO_2 sample were studied.

A γ-ray source of ^{99}Rh in a ruthenium metal matrix was used. All measurements were performed at liquid helium temperature.

Results

(i) *Ruthenium in titanium dioxide*

Figure 5.1.1 shows the Mössbauer absorption spectra obtained for the ruthenium doped titanium dioxide sample for $\gamma \| [001]$ and $\gamma \| [100]$. The spectra have been fitted by a theoretical equation for a single quadrupole doublet in which the quadrupole splitting of the excited state, the isomer shift, and the angle between the γ-rays and the principal EFG axis are allowed to vary. The quadrupole splitting of the ground state is a known fraction of the excited state splitting [81]. In our fit the EFG is taken to be axially symmetric which means that the three perpendicular components V_{xx}, V_{yy} and V_{zz} are related by the equation $V_{xx} = V_{yy} = \frac{1}{2}V_{zz}$. The relative intensities of the six components are known functions of the angle between the γ-ray direction and the principal axis of the EFG [83].

The best fit for the spectrum with $\gamma \| [001]$, giving the solid line shown in Fig. 5.1.1 is obtained using an isomer shift of $-0.268(10)$ mm/s, a positive electric field gradient ($V_{zz} > 0$) with a quadrupole splitting (eQV_{zz}) of 0.556(10) mm/s (where Q is the quadrupole moment of the excited state), and an angle of 90° between the γ-ray direction and the EFG axis.

The best fit for the $\gamma \| [100]$ spectrum is obtained for an isomer shift of $-0.283(10)$ mm/s, a quadrupole splitting of $+0.589(10)$ mm/s and an angle of 45° between the γ-ray direction and the EFG axis.

Both spectra can therefore be accurately fitted by a single quadrupole doublet, assuming an axially symmetric EFG. The differences between the isomer shift and quadrupole splitting values found for the two different orientations are of the same order as the experimental uncertainty, but could possibly be reduced slightly if an asymmetric EFG ($V_{yy} \neq V_{xx}$) were used. A positive EFG along the

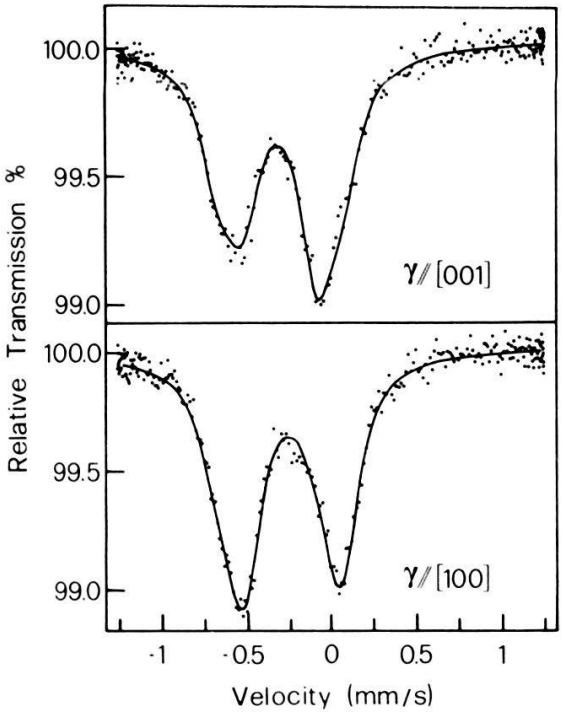

Figure 5.1.1
Mössbauer absorption spectra of Ru doped TiO_2 with the γ-ray direction parallel to [001] and [100].

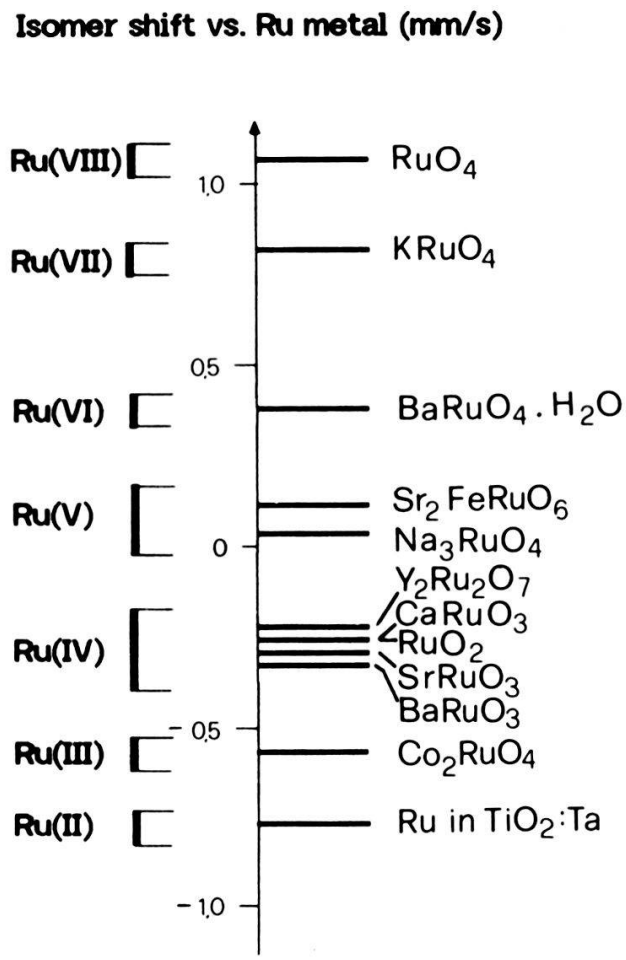

Figure 5.1.2
^{99}Ru isomer shifts for Ru oxides in different valence states. Data is from this work and Ref. 82.

[110] or [1$\bar{1}$0] axis, corresponding to the principal axes of the oxygen octahedra at the two non equivalent cation sites is compatible with both spectra.

In Fig. 5.1.2 we show some measured values for isomer shifts of ruthenium oxides. The variation of isomer shift with valence state is clear. The mean value of −0.275 mm/s for our sample is typical of tetravalent ruthenium, and we deduce that virtually all the ruthenium in our sample is present in this valence state.

In Fig. 5.1.3 we show the spectra obtained for the rutile sample containing 1.0% ^{99}Ru and 0.3% Ta, again for $\gamma \| [001]$ and $\gamma \| [100]$. The spectra also resemble quadrupole doublets, and the variation of the relative intensities of the two peaks with orientation is the same as for the sample doped only with ruthenium. For both orientations, however, the peak near −0.5 mm/s is significantly stronger for the sample containing tantalum. In adddition this peak is wider, and displaced slightly to more negative velocities. If this peak is fitted by a Lorentzian curve in each spectrum of Figs. 5.1.1 and 5.1.3 we obtain a mean peak position of −0.553(3) mm/s and width 0.300(5) mm/s for the sample doped only with ruthenium, and a position of −0.564(3) mm/s and width 0.405(5) mm/s for the sample with added tantalum. This is evidence that as well as the quadrupole doublet of tetravalent ruthenium, the spectra in Fig. 5.1.3 contain an additional structure situated near −0.6 mm/s. In Fig. 5.1.2 this corresponds well with the isomer shift of trivalent ruthenium, and implies that addition of tantalum has converted some of the Ru^{4+} to Ru^{3+}.

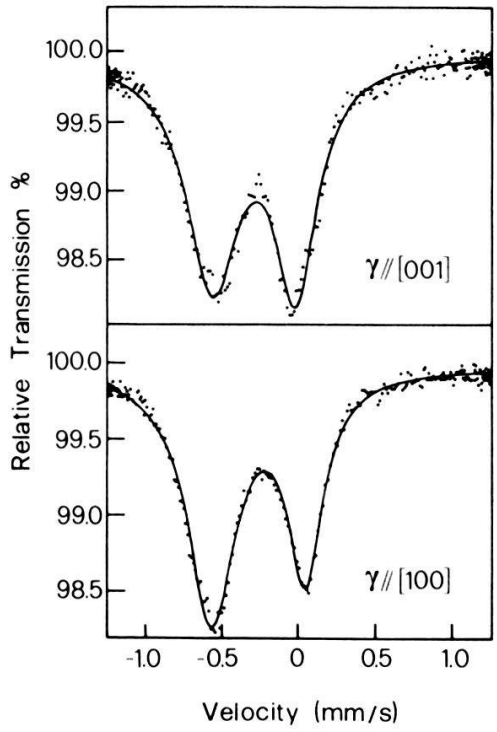

Figure 5.1.3
Mössbauer absorption spectra of TiO_2 containing 0.3% Ta and 1% ^{99}Ru with the γ-ray direction parallel to [001] and [100].

In Fig. 5.1.4 we show the spectrum of a polycrystalline sample of ruthenium doped with 1% Ru and 1.5% Ta. We observe three peaks, at −0.01(2), −0.45(2) and −0.76(2) mm/s. The peak near zero velocity corresponds well in position to one peak of the tetravelent ruthenium spectrum. We also see a peak near −0.5 mm/s which is the expected position of the second peak of the doublet. In a polycrystalline sample however the two peaks of a doublet should have equal intensities, and the strength of the peak at −0.45 mm/s suggests that an additional contribution is present near −0.6 mm/s. This implies that a certain amount of trivalent ruthenium is present in the sample. The strong peak at −0.76 mm/s was completely absent in the sample containing less tantalum (Fig. 5.1.3), and infers that ruthenium is also present in a lower valence state than three. Although a negative isomer shift of this strength has not previously been observed for an

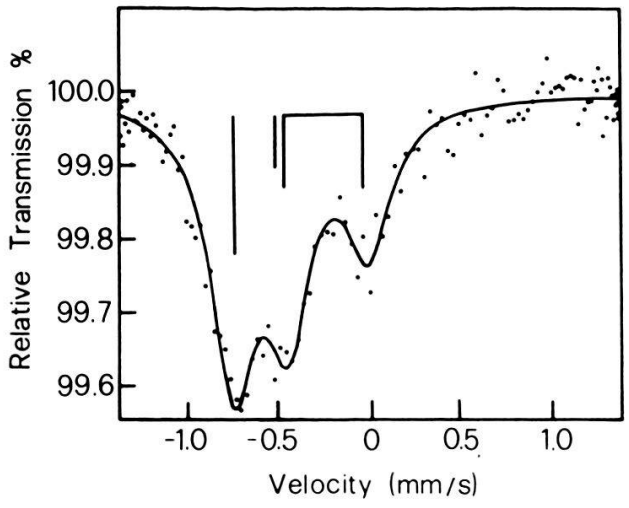

Figure 5.1.4
Mössbauer absorption spectrum of polycrystalline TiO_2 doped with 1% Ru and 1.5% Ta.

oxide of ruthenium, we deduce by extrapolation of the data in Fig. 5.1.2 that this peak must be due to divalent ruthenium.

(ii) *Ruthenium dioxide*

Although a number of studies of the Mössbauer absorption of RuO_2 have been performed [84], allowing the isomer shift and strength of the quadrupole splitting to be deduced, neither the sign nor the orientation of the EFG have been found.

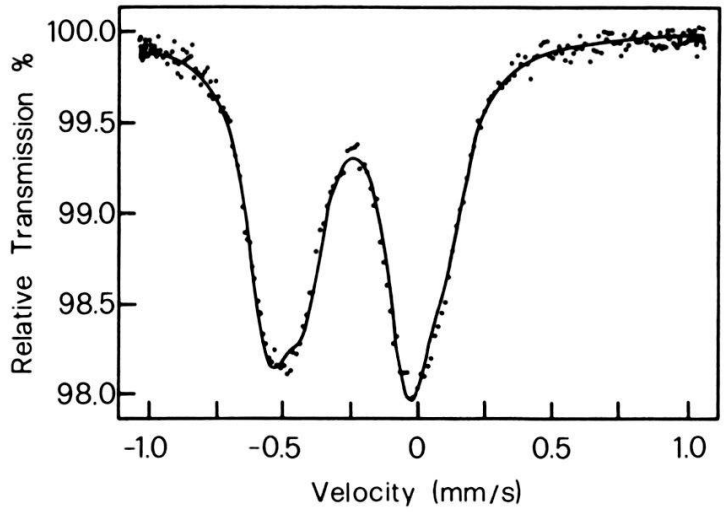

Figure 5.1.5
Mössbauer absorption spectrum of polycrystalline RuO_2.

Figure 5.1.5 shows the spectrum of a polycrystalline RuO_2 sample. The continuous line shows the theoretical fit assuming an axially symmetric EFG. The best fit is obtained using an isomer shift of $-0.252(5)$ mm/s, and $eQV_{zz} = -0.525(5)$. Figure 5.1.6 then shows the measurement on a single crystal sample with the γ-ray direction parallel to [001]. The isomer shift and quadrupole splitting for the best fit are $-0.264(7)$ and $-0.551(10)$ mm/s respectively, and the

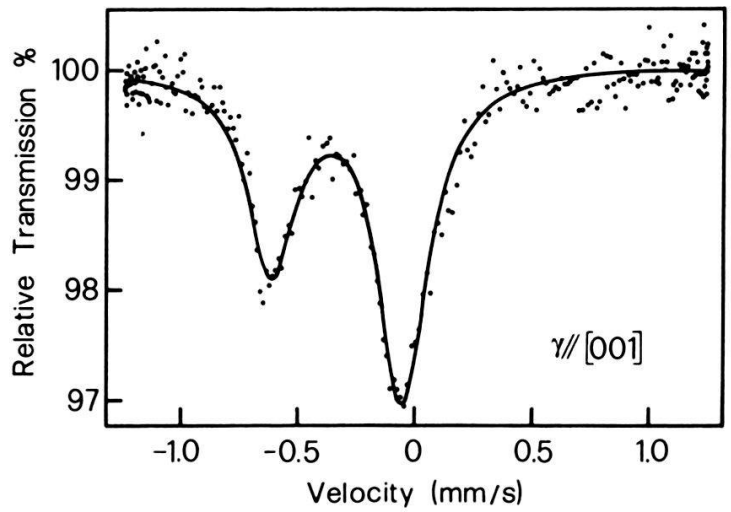

Figure 5.1.6
Mössbauer absorption spectrum of a RuO_2 single crystal with the γ-ray direction parallel to [001].

EFG direction is found to be [001]. As for Ru in titanium dioxide, the disagreement in the isomer shift and quadruopole splitting between the two measurements is small showing that the EFG is nearly axially symmetric. This study is continuing, and will be reported later [85] when measurements with $\gamma \| [110]$ will also be available. The present results show however that the principal axis of the EFG is along [001], and that in this direction the field gradient is negative.

Conclusions

We have measured the Mössbauer absorption of the 89.4 keV γ-ray of ^{99}Ru in samples of ruthenium doped titanium dioxide, and in ruthenium dioxide. The measurements have shown that ruthenium replaces Ti^{4+} substitutionally in rutile as Ru^{4+}. On addition of small amounts of tantalum to the system an enhancement of the absorption spectrum occurs near -0.6 mm/s implying that some Ru^{4+} is converted to Ru^{3+}. In a sample containing more tantalum than ruthenium a strong signal is observed which can be attributed to Ru^{2+}.

An analysis of the spectra of tetravalent ruthenium in TiO_2 reveals that the electric field gradient at the ruthenium nucleus is positive and lies along the main axis of the oxygen octahedron surrounding the cation, that is in a [110] direction. A similar analysis applied to ruthenium dioxide indicates that the principal axis of the EFG lies in the [001] direction, and that the EFG in this direction is negative. In both cases therefore the EFG in the [110] direction is positive, and in the [001] direction is negative. For Ru in TiO_2 the former is stronger while in RuO_2 the latter is stronger. The origin of this difference probably lies in the difference in lattice parameters in these materials.

5.2. Electron Paramagnetic Resonance

Electron Paramagnetic Resonance (EPR) induces transitions between different energy levels of a paramagnetic body by the application of a high frequency electromagnetic field, in the presence of a static magnetic field. The technique is particularly appropriate for the study of impurities in solids. The energy levels of the impurity are described by a spin Hamiltonian which depends on the impurity itself, and its environment in the crystal. The measurements often allow the identification of the impurities present in the solid, their valence state, and the local symmetry, which may allow the site itself to be identified.

We report here the results of an EPR study at 13 and 19 GHZ at 4.2 K, of a titanium dioxide (rutile) sample doped with 0.02% Ru in a fully oxidised state, and then reduced in Formier gas (94% N_2, 6% H_2) at various temperatures up to 800°C. A second crystal containing 0.1% of both Ru and Ta has also been examined. Both samples were grown by chemical vapour transport using $TeCl_4$ [72].

Mössbauer studies [5.1] have shown that ruthenium replaces titanium substitutionally in fully oxidised rutile, mainly in the tetravalent state. On codoping with tantalum a clear signal due to divalent ruthenium was observed, but some doubts remained as to the existence of trivalent ruthenium in rutile.

In the strong crystal field present at the cation site in rutile, the tetra- and

divalent ruthenium ions have the diamagnetic (t_{2g}^4) $^3T_1$ and (t_{2g}^6) $^1A_1$ ground states and cannot be observed by EPR. Trivalent ruthenium has been observed in TiO_2 powders by Valigi et al. [86]. We have observed this spectrum, and a new spectrum which we attribute to pentavalent ruthenium. Rutile TiO_2 has a tetragonal crystal structure [2.1]. The cations lie at the centre of a slightly distorted octahedron of oxygen ions. Two sites exist which differ by a rotation of about 90° about the c-axis. The principal axis of the octahedron which we denote by y lies along [110] for half the cations, and along $[1\bar{1}0]$ for the other half. The sites are equivalent when the magnetic field lies along the [001] c-axis which we denote by z. The third axis of the site is denoted by x, and lies along $[1\bar{1}0]$ or [110].

Results

Figure 5.2.1 shows the spectrum of the fully oxidised ruthenium doped rutile sample recorded at 13 GHz, with the magnetic field parallel to the [110] direction. Two spectra are shown, centred at 3291.3 and 3461.8 Gauss. Both spectra can be attributed to ruthenium because they exhibit the characteristic hyperfine interaction with the ^{99}Ru and ^{101}Ru nuclei having spin $I = \frac{5}{2}$ and natural abundancies of 12.7 and 17.1%. This interaction produces the weak satelite lines disposed symmetrically around the central peak, as observed for trivalent ruthenium in MgO by Raizman et al. [87]. The angular variation of the central component of each signal in the (110) and (001) planes is shown in Fig. 5.2.2. Both signals are generated on two sites which differ by a 90° rotation about the c-axis, and the angular dependence in both cases is compatible with ions substituting for titanium on regular cation sites.

The sample doped with 0.1% of both Ru and Ta showed only one signal, identical in form and angular dependence to the weaker signal in Fig. 5.2.1, but significantly stronger. The signal in this sample is expected to be due to a low valency like three because of the compensating effect of the pentavalent tantalum.

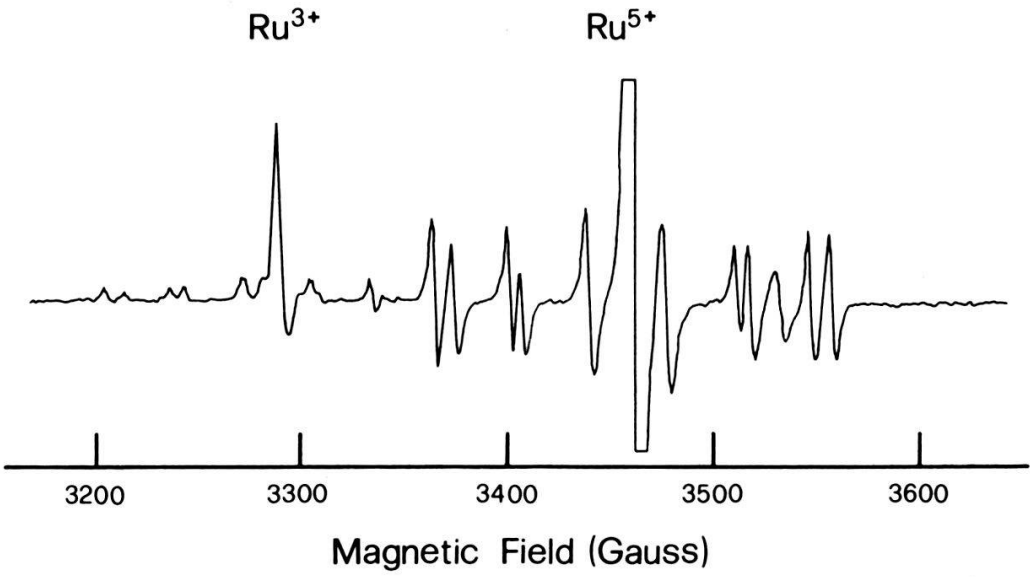

Figure 5.2.1
EPR Spectrum of Ru doped TiO_2 single crystal along [110] showing two distinct spectra. Both can be attributed to Ru because of the characteristic hyperfine interaction.

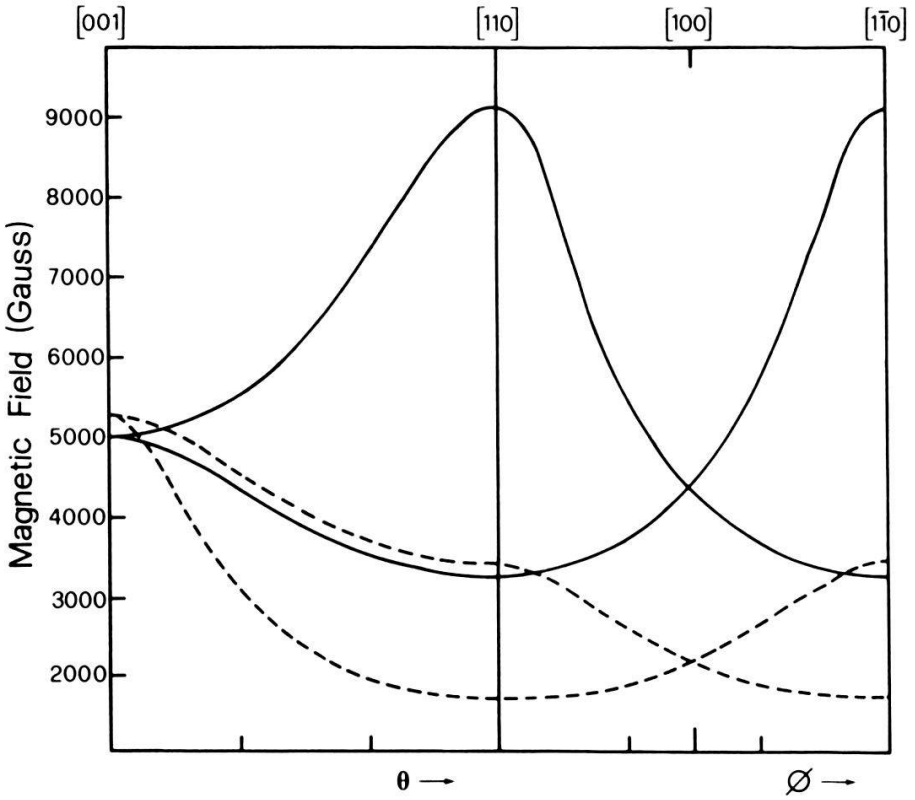

Figure 5.2.2
Angular variation of Ru EPR spectra in TiO_2. The dottted line shows the spectrum attributed to Ru^{5+} and the continuous line the spectrum attributed to Ru^{3+}.

Reduction of the Ru doped crystal in hydrogen is also expected to lower the ruthenium valency [65]. Reduction at 500°C increased the strength of the weaker signal in Fig. 5.2.1, while the stronger signal became very weak. For this reason we attribute the stronger signal to pentavalent ruthenium, and the weaker signal to trivalent ruthenium. Reduction at 800°C destroyed all Ru signals, and only the A spectrum reported by Chester [24] in reduced rutile was observed.

The $4d^5$ electron configuration of the trivalent ruthenium ion in the strong crystal field at the centre of an oxygen octahedron is in the low spin $(t_{2g}^5)\ ^2T_2$ state with $s = \frac{1}{2}$ and $1 = 1$ coupled to give a total spin $S = \frac{1}{2}$. The spectrum assigned to Ru^{3+} can be accurately described by the following spin Hamiltonian for a $S = \frac{1}{2}$ centre.

$$H = \mu g_z s_z H_z + \mu g_x s_x H_x + \mu g_y S_y H_y + A_z S_z I_z + A_x S_x I_x + A_y S_y I_y$$

where $g_z = 1.845$, $g_x = 2.822$, $g_y = 1.015$, in close agreement with Valigi et al. [86]. The hyperfine splitting could not be resolved with $H \parallel z$ so A_z could not be determined. The values found for A_x and A_y are given in Table 5.2.1.

The mean g value of 1.89 gives an orbital angular momentum reduction factor k of 0.78 which is significantly larger than measured values for tetravalent d^5 ions in similar environments. This will be discussed in more detail in a future publication [88].

The $4d^3$ Ru^{5+} ion is expected to be in the $(t_{2g}^3)\ ^4A_2$ state with spin $S = \frac{3}{2}$. For a spin $= \frac{3}{2}$ state the Hamiltonian contains additional spin dependent crystal field terms.

Table 5.2.1
Spin Hamiltonian and hyperfine parameters for Ru^{3+} and Ru^{5+} in rutile. Units are cm^{-1} for D and E, and $10^{-4}\,cm^{-1}$ for the components of A.

Ion	g_x	g_y	g_z	D	E		A_x	A_y	A_z
Ru^{3+}	2.822	1.015	1.845	—	—	^{99}Ru	34.0	26.3	—
						^{101}Ru	38.1	30.2	—
Ru^{5+}	1.62	2.28	1.82	3.0	0.16	^{99}Ru	66.6	37.3	22.2
						^{101}Ru	75.7	42.6	25.5

In an orthorhombic crystal field the Hamiltonian becomes:

$$H = \mu g_z S_z H_z + \mu g_x S_x H_x + \mu g_y S_y H_y + A_z S_z I_z - A_x S_x I_x + A_y S_y I_y + D[S_z^2 - S(S+1)/3)] + E(S_x^2 + S_y^2)$$

Starting values for the fit were obtained from the expression of Geusic et al. [89] using a tetragonal field approximation. This approximation can be used to describe the spectrum when the magnetic field lies in the [100] or [010] directions. In this case the term containing E does not contribute. Measurement of the resonance field of the $+\frac{1}{2}$ to $-\frac{1}{2}$ transition at two different frequencies (13 and 19 GHz in this case, shown as 1 and 2) allows $g_\perp$ and D to be determined from:

$$g_\perp = 0.5\ g_\perp(1)\ (1/\alpha)((\alpha - \delta)/(1-\delta))$$
$$D = g_\perp \mu (\tfrac{3}{4}(\alpha H(2)^2 - H(1)^2)/(\alpha - 1))^{1/2}$$

where $\delta = (H(1)/H(2))^2$ and $\alpha = g_\perp(1)/g_\perp(2)$.

The best fit for the hamiltonian was obtained with $g_x = 1.62$, $g_y = 2.28$, $g_z = 1.82$, $D = 3.0\,cm^{-1}$ and $E = 0.16\,cm^{-1}$. The hyperfine splitting was resolved in all directions for the Ru^{5+} ion, and the hyperfine parameters are shown in Table 5.2.1.

Conclusions

We have observed EPR signals of two different ruthenium centres substituting for titanium in TiO_2. One has spin $\frac{1}{2}$ and from its dependence on reduction and donor doping we identify it as Ru^{3+}. The other has spin $\frac{3}{2}$ and is observed in fully oxidised ruthenium doped titanium dioxide, but not in reduced or donor doped samples. We identify this centre as Ru^{5+}. These results, together with the Mössbauer spectroscopy [5.1] show that all four valence states of ruthenium from pentavalent to divalent are stable in rutile, depending on the position of the Fermi level in the band gap.

5.3. Optical properties

While the Mössbauer and EPR measurements described above have allowed the stable valence state of ruthenium in titanium dioxide to be identified as a function of donor doping and reduction, they give no information on the energies of these states, or on the presence of free carriers.

In this section we present optical absorption spectra of TiO_2 doped with Ru

alone, and with both Ru and the donor Ta. We also present optical absorption spectra of Ru doped TiO_2 after reduction in vacuum, and in hydrogen at successively higher temperatures. Absorption bands are observed which can be attributed to acceptor transitions of the Ru^{4+} ion, and to donor transitions of the Ru^{3+} and Ru^{2+} ions.

Donor doping is shown to convert the ruthenium to Ru^{3+} and Ru^{2+} before free carriers appear. Reduction in hydrogen converts the ruthenium to Ru^{3+} and then Ru^{2+}, and further reduction leads to the formation of defect complexes with intense absorption bands. Reduction in vacuum converts all ruthenium to Ru^{3+} but only partial reduction to Ru^{2+} occurs before complex formation followed by precipitation of the ruthenium from the lattice.

Experimental

All doped samples used in this investigation were grown by chemical vapour transport using $TeCl_4$ as transport agent [72]. All dopant concentrations given correspond to the concentration in the source material used for crystal growth. Actual concentrations in crystals are estimated to be within 20% of this figure. Plates for transmission measurements were obtained by polishing the crystals parallel to a natural face. In this way (111), (110) or (100) slices were obtained. (110) slices proved to be extremely fragile and were avoided when possible. The plates used for transmission measurements were (100) for stoichiometric ruthenium doped titanium dioxide samples doped with less than 0.1% Ru, and (111) for the other samples, including the 0.02% Ru sample used for vacuum and hydrogen reduction. The samples doped with both Ru and Ta or Nb were all (111) plates except the 0.1% Ru, 0.4% Ta sample which was (110). The pure titanium dioxide sample was a (001) plate cut from a flame fusion boule supplied by Djevahirdjian, Monthey, Switzerland.

The absorption coefficient α can be obtained from the transmission coefficient T and the reflectivity R from the expression:

$$T = \frac{(1-R)^2 e^{-\alpha d}}{1-R^2 e^{-2\alpha d}}$$

In most cases the term $R^2 e^{-2\alpha d}$ was insignificant and therefore neglected. The reflection coefficient was taken from Cardona and Harbeke [15] for light polarised parallel or perpendicular to the optical axis. Our own data for R was used for measurements with unpolarised light. Measurements of R at room temperature showed only minor variations with doping, and it was considered sufficient to use the reflection coefficient of pure TiO_2. In the domain where the absorption coefficient is close to zero we eliminated R by measuring T for two different sample thicknesses. Transmission measurements in the visible range on Ru doped TiO_2 were performed on a home-made spectrometer using two EMI 9659QB photomultipliers, but all other measurements were made using a Beckmann Acta M VII spectrometer.

Vacuum reduction was performed at 10^{-7} Torr, using a cryogenic pump – ionisation pump system to avoid oil contamination. Hydrogen reduction was performed in flowing hydrogen, and the temperature was measured near the

sample but outside the hydrogen tube. The real sample temperature during reduction was probably slightly lower than the temperature indicated because of incomplete heating of the hydrogen before it reached the sample.

Results

(i) *Ru doped TiO_2*

Absorption spectra of Ru doped TiO_2 samples with Ru concentrations varying from zero to 2% are presented in Fig. 5.3.1. The absorption coefficient of pure TiO_2 is nearly zero at sub band-gap energies, and increases very steeply with energy above three electron volts. Doping with increasing amounts of Ru leads to the appearance of an absorption band beginning around 2 eV, and extending to the fundamental edge at 3 eV. In samples where the fundamental edge is visible, we note that the slope of the Ru absorption band decreases about 2.8 eV, suggesting that this band reaches a maximum just above 3 eV. In Fig. 5.3.2 we see that for the more strongly doped samples, a small peak is clearly visible at 1.85 eV.

The polarisation dependence of the absorption coefficient (α) was measured on four samples with concentrations ranging from 0.02% to 2% Ru. The same dependence was found in the four cases. The inset in Fig. 5.3.1 shows the polarisation dependence for the 0.07% Ru sample. We note that α is significantly higher parallel to the optical axis. The small peak at 1.85 eV does not show a strong polarisation dependence.

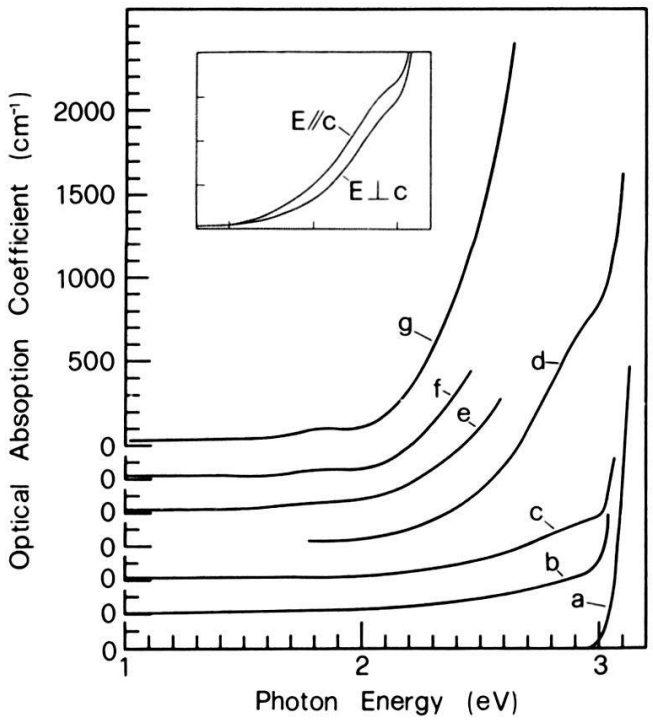

Figure 5.3.1
Optical absorption spectra of Ru doped TiO_2 at 300 K. The samples contain the following Ru concentrations in atomic percent. (a) 0, (b) 0.005, (c) 0.02, (d) 0.07, (e) 0.1, (f) 0.2, (g) 2. The polarisation dependence of the absorption is shown in the inset.

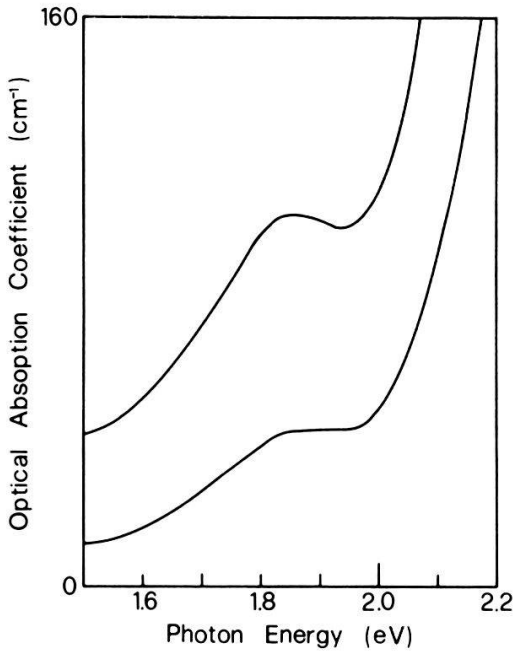

Figure 5.3.2
Enlarged spectra of the two most strongly doped samples showing structure at 1.85 eV.

The absorption spectrum of the 0.02% Ru sample was measured at 2 K, at 77 K and at room temperature. No significant variation with temperature in either the 1.85 eV peak or the 2–3 eV band was observed.

From the Mössbauer measurements in Section 5.1, we know that nearly all the Ru in these samples in present as Ru^{4+}. The absorption bands observed can therefore be assigned to transitions involving this ion. The transitions which could produce absorption in this energy range are internal $d-d$ transitions of the Ru^{4+} ion, or charge transfer transitions of the donor ($Ru^{4+} \rightarrow Ru^{5+} + e^-$) or acceptor ($Ru^{4+} \rightarrow Ru^{3+} + h^+$) type. The cation site in TiO_2 is a centre of symmetry. Internal $d-d$ transitions of a cation are therefore forbidden, and can be expected to give rise to absorption bands orders of magnitude weaker than charge transfer bands.

Ru^{4+} is in an almost identical site in RuO_2. Goel et al. [54] calculated the imaginary part of the refractive index of RuO_2 from reflectivity measurements. The first charge transfer band corresponding to oxygen 2p to ruthenium 4d t_{2g} transitions extends from 2 to 4 eV with a maximum at 3 eV of $k \approx 1$, i.e. $\alpha \approx 3 \times 10^5\ cm^{-1}$. In comparison, our sample of TiO_2 doped with 0.07% Ru also absorbs from 2 eV onwards, and just before the intrinsic edge the absorption coefficient is $1.3 \times 10^3\ cm^{-1}$. Taking into account the number of ruthenium ions per unit volume present, the absorption band in our sample is even stronger than the charge transfer band in RuO_2, and we can definitely rule out internal d–d transitions as the cause. The strong band extending from 2 eV to the intrinsic edge must therefore be due to charge transfer transitions. This is supported by recent photoelectrochemical measurements [90, 91] which show that carrier creation in Ru doped titanium dioxide occurs for $h\nu > 2$ eV.

In general it is difficult to distinguish between donor and acceptor transitions of an impurity ion. The matrix element for a transition depends essentially on the overlap between the wavefunctions of the initial and final states. In TiO_2 the valence band is composed of oxygen 2p states, and the conduction band of Ti 3d states. Since each cation is surrounded by an octahedron of oxygen ions, we expect acceptor transitions to be considerably stronger than donor transitions. For

this reason we attribute the strong absorption band observed to acceptor transitions of the Ru^{4+} ion.

The weak band at 1.85 eV could arise from various factors. Possible candidates are internal d–d transitions of ruthenium ions, and the excitation of an electron from one ruthenium ion, to another on a neighbouring cation site. From the form and energy of the band, considering the Ru^{2+} and Ru^{3+} donor transitions discussed later, we rule out donor transitions of the Ru^{4+} ion as the cause.

The polarisation dependence of the Ru^{4+} band in TiO_2 contrasts with that of the O 2p to Ru 4d t_{2g} transition in RuO_2, where after subtraction of the free electron contribution the absorption is stronger perpendicular to the optical axis. This may be related to the fact that in RuO_2 the shortest cation–anion bond lies along [110], whereas in TiO_2 the bond along [110] is longer than the four other cation-anion bonds in the (110) plane.

(ii) *TiO_2 doped with Ru and Ta (or Nb).*

The absorption spectra of a series of samples doped with 0.1% Ru and various Ta concentrations are shown in Fig. 5.3.3. The curves are labelled with the nominal Ta to Ru concentration ratio. The curve representing 0.1% Ru and no Ta has been extended above 2.5 eV using data from the 0.07% Ru sample.

TiO_2 doped with equal amounts of Ta and Ru (curve 1) shows a broad absorption band with maximum around 2.6 eV. Doping with twice as much Ta as Ru (curve 2) produces an absorption band centred at around 1.7 eV. Increasing the Ta concentration further (curve 4) appears to have little effect on this band, but a marked increase in absorption occurs below 1 eV. The broken line shows the difference between curves 4 and 2. The absorption of sample 2 was found to show no significant temperature dependence in the range 25 K to 300 K.

In order to establish that the structure at 2.6 eV is an absorption band, and not a superposition of the band extending from 2 eV to the intrinsic edge, and the broad band centred at 1.7 eV, we have studied linear combinations of these two features. No combination of these bands resembles the 2.6 eV structure, which

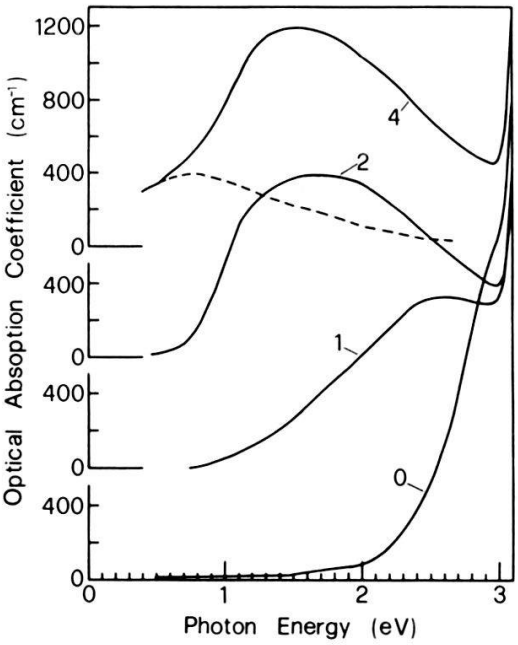

Figure 5.3.3
Optical absorption spectra of TiO_2 samples doped with 0.1% Ru and various amounts of Ta. The labels give the nominal Ta to Ru concentration ratio. The dashed line shows the difference between curves 4 and 2.

must therefore be considered as an independent band, related to a distinct stage in the donor doping series.

As discussed above, the absorption band of the sample with 0.1% Ru and no Ta is associated with the Ru^{4+} ion. All samples doped with both Ru and Ta show weaker absorption just below the fundamental edge than the sample doped only with ruthenium, demonstrating a decrease in the number of Ru^{4+} ions present. From our Mössbauer measurements we know that addition of Ta to Ru doped TiO_2 leads to Ru^{3+}, and Ru^{2+} formation, depending on the relative concentrations. In the sample doped with 0.1% Ru and 0.1% Ta we expect most of the Ru to be present as Ru^{3+}, and a strong Ru^{3+} EPR signal has been observed in a sample with these doping concentrations. We therefore assign the absorption band with maximum at 2.6 eV to transitions involving the Ru^{3+} ion. If this band were due to acceptor transitions it would lie at higher energy than the same band for Ru^{4+}. Since Ru^{4+} shows no absorption at lower energies this cannot be the case. Therefore we attribute this band to donor transitions of the type:

$$Ru^{3+} \rightarrow Ru^{4+} + e^- \text{ (conduction band)}$$

Most ruthenium in the sample doped with 0.1% Ru and 0.2% Ta should be present as Ru^{2+}. We therefore attribute the absorption band centred at 1.7 eV of this sample to transitions involving this ion. Since this band is at lower energy than the Ru^{4+} and Ru^{3+} absorption bands, it can be attributed to the donor transition:

$$Ru^{2+} \rightarrow Ru^{3+} + e^- \text{ (conduction band)}$$

The sample doped with 0.1% Ru and 0.4% Ta has virtually the same absorption coefficient as the 0.1% Ru, 0.2% Ta sample in the range 2.3 to 3.0 eV. We deduce that the Ru^{2+} population in the two samples is the same. The difference in absorption of the two samples, shown by the dashed line, corresponds well with the free carrier absorption band measured on a TiO_2 sample doped with 0.2% Ta and no Ru. It appears then that when all ruthenium is present as Ru^{2+}, further donor doping is no longer compensated.

We also prepared a sample of TiO_2 doped with 0.1% Ru and 0.2% Nb. Its absorption spectrum is almost identical to that of the 0.1% Ru, 0.2% Ta sample shown in Fig. 5.3.3. This is consistent with the assignment of the 1.7 eV band to Ru^{2+} donor transitions, and the fact that both Ta and Nb behave as shallow electron donors in TiO_2.

(iii) *Effect of reduction in hydrogen on Ru doped TiO_2*

A TiO_2 sample doped with 0.02% Ru was reduced in flowing hydrogen at successively higher temperatures. The sample, $0.15 \times 8 \times 5$ mm, was heated for twenty minutes at each temperature and cooled slowly before the optical spectra were taken. Reduction was first performed at 400°C, and then at fifty degree intervals from 500 to 750°C. Spectra indicating important stages in the reduction are shown in Fig. 5.3.4. The thermogravimetric measurements of Valigi and Gazzoli [65] on Ru doped TiO_2 are shown in Fig. 5.3.5 for comparison. If we consider that our sample temperature during reduction was a few degrees below

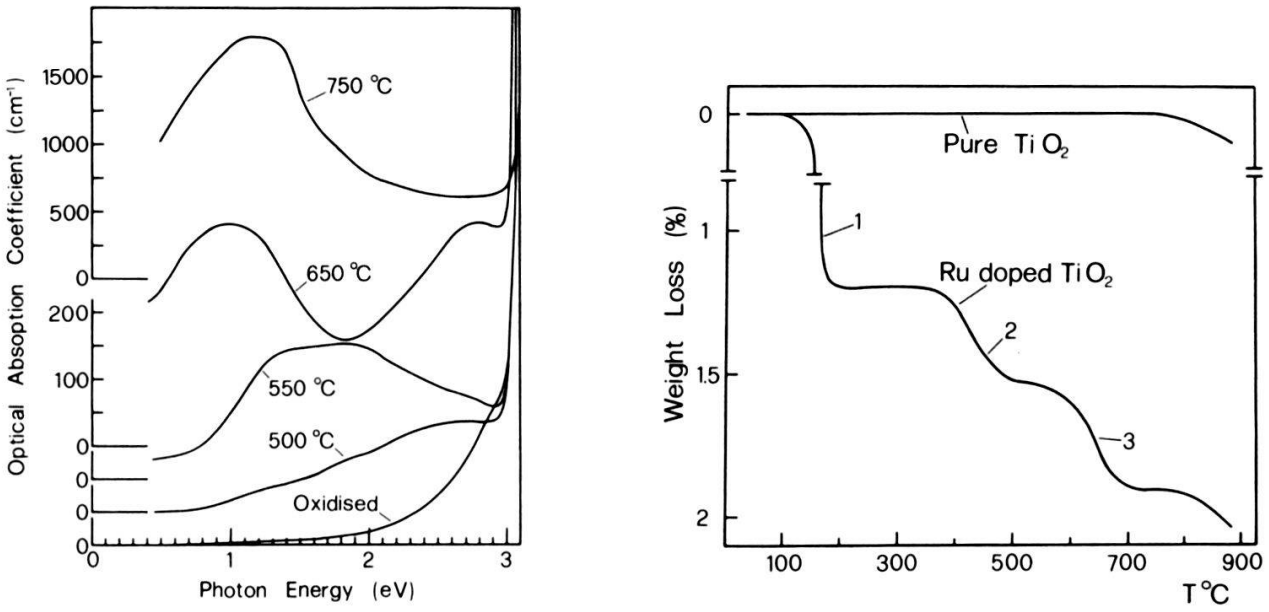

Figure 5.3.4
Optical absoprtion spectra of TiO_2:0.02% Ru as a function of reduction in hydrogen for 20 minutes at successively higher temperatures. Note fivefold scale reduction for 750°C spectrum.
Figure 5.3.5
Weight loss measurements of TiO_2 and Ru doped TiO_2 on heating in hydrogen, from Ref. 65. The steps 1 to 3 are interpreted as 1; Reduction of excess RuO_2 to Ru metal. 2; Reduction of dissolved Ru^{4+} to Ru^{2+}. 3; Reduction of dissolved Ru^{2+} to Ru metal.

the temperature indicated, the five absorption curves in Fig. 5.3.4 correspond to:

(i) Fully oxidised sample containing mostly Ru^{4+}.
(ii) Intermediate stage in Ru^{4+} to Ru^{2+} transition (500°C).
(iii) All ruthenium reduced to Ru^{2+} (550°C).
(iv) Intermediate stage in Ru^{2+} to Ru metal transition (650°C).
(v) All ruthenium reduced to metal (750°C).

In the spectrum of the fully oxidised sample we find the familiar Ru^{4+} absorption band discussed above. The absorption spectrum of the sample reduced at 500°C shows a band starting below 1 eV, with a marked shoulder at 2.7 eV. This band is very similar to that of the TiO_2:0.1% Ru, 0.1% Ta sample (curve 1) in the last section, which we attributed to donor transitions of the Ru^{3+} ion. After reduction at 550°C the sample shows a band with a flat top extending from 1.3 to 1.9 eV. This band strongly resembles that of the TiO_2:0.1% Ru, 0.2% Ta sample attributed to donor transitions of the Ru^{2+} ion. After reduction at 600°C the sample absorbed more strongly below 1.3 eV and above 1.9 eV giving a rather flat spectrum. This evolution continued on reduction at 650°C, after which the absorption spectrum shows two strong bands with maxima around 0.9 and 2.8 eV. The absorption coefficient at 1.9 eV is actually lower than in the 550°C spectrum, indicating that the Ru^{2+} population has decreased. Reduction at 700°C leads to increased absorption at all wavelengths, and after reduction at 750°C we find a single strong peak at 1.2 eV (note fivefold scale reduction in Fig. 5.3.4).

The similarity between the absorption spectrum of the sample after reduction at 550°C, and that of the TiO_2:0.1% Ru, 0.2% Ta sample is consistent with the

measurements of Valigi which indicate that Ru doped TiO_2 reduced at this temperature in hydrogen should contain mostly Ru^{2+}. As in the last section for curve 1, the absorption band of the sample reduced at 500°C cannot be obtained by a linear combination of the Ru^{2+} and Ru^{4+} bands, and we conclude that most ruthenium in the sample must be present as Ru^{3+}. This implies that the Ru^{4+} to Ru^{2+} step observed in the thermogravimetric measurements is composed of the two distinct steps, Ru^{4+} to Ru^{3+}, and Ru^{3+} to Ru^{2+}, but that these were not resolved. As mentioned above a strong EPR signal from substitutional Ru^{3+} has been observed in a Ru doped TiO_2 sample reduced in hydrogen at 500°C.

The spectra obtained after reduction at 650°C and above are not well understood. We expect the ruthenium to be partially transformed from Ru^{2+} to Ru metal at 650°C, and completely transformed at 750°. Valigi [65] found that this process involves precipitation of the ruthenium from the rutile lattice. Their sample contained around 1.8 mol% ruthenium however, which is close to the solubility limit of Ru^{4+} in TiO_2. As our sample contains only 0.02% ruthenium, segregation is less probable, and the absorption spectrum after reduction at 750°C indicates that it does not take place to an appreciable extent. The reduction of isolated ruthenium ions to Ru^{+} or Ru^{0} may occur via the formation of complexes involving structural defects, probably oxygen vacancies. The formation of such complexes has been observed for aluminium in TiO_2 by Kersson and Volger [31]. We therefore attribute the strong absorption bands obtained on reduction at 650°C and above to charge transfer transitions of point defect – ruthenium ion complexes. Similar behaviour for a variety of transition metal ions in $SrTiO_3$ has been recently reported by Blazey and Weibel [92].

(iv) *Effect of Vacuum Reduction on Ru doped TiO_2*

Before hydrogen reduction, the TiO_2 sample doped with 0.02% Ru was reduced in vacuum at various temperatures from 800 to 960°C. The sample was heated for two hours at each temperature and cooled slowly before the optical spectra were measured. Figure 5.3.6 shows absorption spectra obtained at various stages of reduction. In the spectrum of the fully oxidised sample we find the familiar Ru^{4+} band. Heating at 800°C leads to a slight shift of the absorption band to lower energies, and at 850°C a marked shoulder appears at 2.7 eV. The spectrum at this stage is similar to curve 1 of Fig. 5.3.3, and the 500°C curve of Fig. 5.3.4, and probably represents a sample with both Ru^{4+} and Ru^{3+} ions present. After reduction at 880°C a decrease in absorption from 2.7 to 3 eV occurs signifying the disappearance of Ru^{4+}, and leaving a well pronounced peak at 2.7 eV which we interpret as the Ru^{3+} donor peak discussed in the last section. Structure has also appeared at lower photon energies, and if we subtract the 850°C spectrum from the 880°C spectrum we find the band shown as a broken line in Fig. 5.3.6 with a peak at 1.3 eV, and a shoulder at 2.0 eV. This structure is probably due to the presence of some Ru^{2+}. On reduction at 920°C we see an increase in absorption below 1 eV combined with a weakening of the absorption between 1.4 and 1.9 eV, and the appearance of a relatively sharp peak at 2.8 eV. This evolution continues on reduction at 960°C, after which the sample shows a peak at 0.8 eV, and a strong peak at 2.8 eV, but the Ru^{2+} absorption band has completely disappeared. Further prolonged reduction at 960°C leads to a weakening of both the 0.8 eV and the 2.8 eV peaks. The sample was then oxidised in

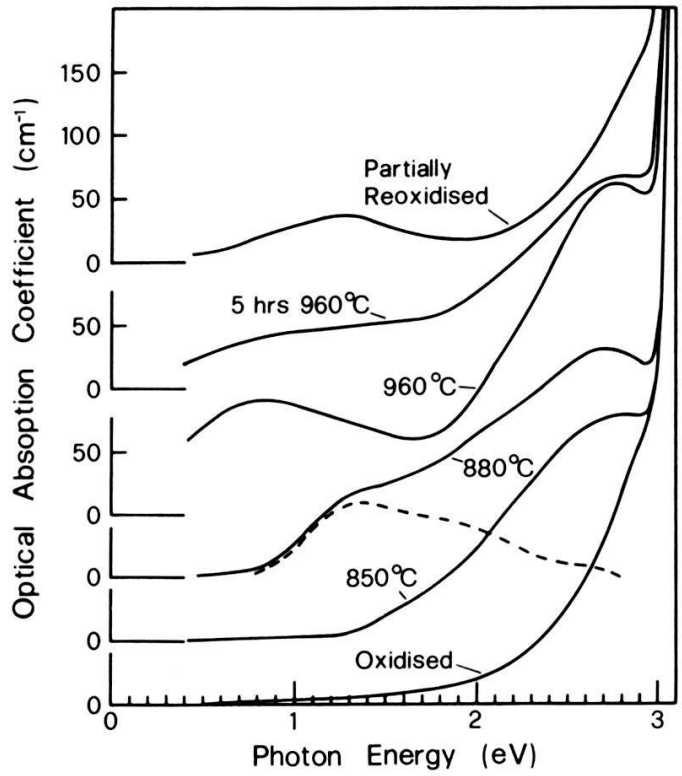

Figure 5.3.6
Optical absorption spectra of TiO_2:0.02% Ru as a function of reduction in vacuum at successively higher temperatures. Reduction time is 2 hrs at each temperature unless indicated. The dashed line shows the change in absorption after reduction at 880°C.

flowing oxygen at 900°C for 3 hours. This gave a spectrum with a weak peak at 1.3 eV, and a band starting at 2 eV, identifiable as the Ru^{4+} band, although slightly weaker than in the original spectrum. Oxidation for a longer period eliminated the peak at 1.3 eV, and the Ru^{4+} band was restored to its initial intensity.

We deduce that the initial effect of vacuum reduction on Ru doped titanium dioxide is to reduce the substitutional Ru^{4+} to Ru^{3+}, and partial reduction to Ru^{2+} occurs at 880°C. Higher temperature vacuum reduction does not convert all the Ru^{3+} to Ru^{2+} however. The sharp peak which appears at 2.8 eV on reduction at 960°C is similar to that observed after reduction in hydrogen at 650°C, and may be due to point defect–Ru ion complexes.

Prolonged reduction at 960°C causes precipitation of the ruthenium from the TiO_2 lattice. A second TiO_2:0.02% Ru sample reduced under identical conditions, and showing the same absorption spectrum has been examined by Transmission Electron Microscopy. Ruthenium precipitates around 200 Angstroms long, and a few atomic layers thick were observed, lying on a family of planes in the TiO_2 lattice. Diffuse reflection by the precipitates is mainly responsible for the absorption spectrum obtained after this treatment. The spectra obtained on reoxidation indicate that full reoxidation to Ru^{4+} in solid solution occurs.

Discussion

Care must always be taken in interpreting optical absorption spectra of impurity ions in titanium dioxide. This fact emerges from studies of Fe, Cr, V and

Mn doped TiO_2 [35, 48, 93]. In most cases, doping requires charge compensation, and this usually occurs by defect formation. Charge transfer transitions of the dopant species may then be obscured by transitions from defects or defect complexes, and defect related absorption bands are often much more intense than the acceptor or donor absorptions of the impurity ions.

In this study we have considered the doping of titanium dioxide by ruthenium. Ruthenium can substitute for Ti^{4+} as Ru^{4+} and it therefore requires no charge compensation. Some Ru^{5+} and Ru^{3+} are present in fully oxidised Ru doped TiO_2, presumably to compensate respectively substitutional trivalent impurities, and interstitial metal ion impurities. However, as shown by Mössbauer measurements the vast majority of ruthenium ions in oxidised TiO_2 are Ru^{4+}, and the optical absorption spectra can be interpreted in terms of charge transfer transitions of this ion.

We have also considered TiO_2 doped with both Ta and Ru, and the effect of reduction on Ru doped TiO_2. Ta is known to behave as a shallow electron donor in TiO_2, and we know from Mössbauer and EPR measurements that the donated electrons are trapped by ruthenium ions, which become Ru^{3+} or Ru^{2+} depending on the relative concentrations of donor to ruthenium. These valence changes are sufficient to compensate entirely the presence of Ta, for Ta to Ru ratios of 2 : 1 or less, without invoking the presence of other charge compensation defects. EPR spectra have shown that the Ru^{3+} ions in TiO_2:0.1% Ru, 0.1% Ta are in undisturbed cation sites. For this reason we feel that the absorption band found in this sample, with its maximum at 2.6 eV can safely be interpreted as being due to donor transitions of the Ru^{3+} ion. We also know from EPR, that reduction of Ru doped TiO_2 in hydrogen at 500°C produces substitutional, undisturbed Ru^{3+} ions. The absorption spectrum of this sample is almost identical to the Ta doped sample, as is the spectrum of the sample reduced in vacuum at 850°C. We can therefore rule out a contribution by Ta or by oxygen vacancies to the absorption band.

In our TiO_2:0.1% Ru, 0.2% Ta sample we expect all ruthenium to be present as Ru^{2+} The absorption spectrum of this sample shows a single broad band centred at 1.7 eV. Evidence that tantalum does not directly contribute to this band comes from the almost identical spectrum of a TiO_2:0.1% Ru, 0.2% Nb sample. The same absorption band is also found in Ru doped TiO_2 after reduction in hydrogen at 550°C, a treatment which according to Valigi reduces all ruthenium to Ru^{2+}. We therefore feel that the absorption band centred at 1.7 eV found in these samples can be attributed to Ru^{2+} donor transitions.

It is interesting to note that donor doping beyond the stage at which all ruthenium is present as Ru^{2+} produces free carriers. (This is confirmed by the electrical measurements in Section 5.4.) In contrast, reduction in hydrogen reduces the ruthenium beyond the Ru^{2+} stage, and complexes of Ru^{+} and Ru^{0} associated with structural defects are probably formed. Reduction in vacuum reduces only part of the ruthenium present to Ru^{2+} before formation of defect complexes occurs. The difference between the effect of reduction in hydrogen, and that of reduction in vacuum may be partly due to the higher temperatures used for vacuum reduction. However, reduction in hydrogen also results in the introduction into the lattice of interstitial hydrogen donors (we observed the O–H bond absorption line at 3030 nm in some of our spectra). This may explain why hydrogen reduction, like donor doping, reduces all ruthenium to Ru^{2+} whereas vacuum reduction does not.

5.4. Electrical properties

From our Mössbauer, EPR and optical studies, it has become clear that ruthenium compensates both donor and acceptor impurities in rutile. It can therefore be expected to influence the number of free carriers induced in this material by donor doping or reduction. We have decided to subject ruthenium doped titanium dioxide to a treatment which normally renders rutile a good n-type semiconductor, and to characterise the electrical conductivity of the material after these treatments.

Although TiO_2 can be made n-type both by doping with donors and by reduction, working with doped as opposed to reduced samples presents distinct advantages. The reasons for this are twofold. Firstly, previous studies have shown that it is difficult to prepare reduced rutile with a conductivity and departure from stoichiometry defined in advance, whereas donor doping gives samples whose point defect and free electron concentrations are well defined [94]. Secondly, we wish to measure the conductivity at high temperature in order to observe effects due to deep impurity levels. Reduced samples are unstable at high temperature and depending on the environment would become more or less stoichiometric during the measurement. In contrast, fully oxidised doped samples are stable at high temperature in an oxidising environment.

We have therefore chosen to investigate the electrical conductivity of a series of fully oxidised samples of TiO_2, doped with a fixed amount of ruthenium and various amounts of the donor tantalum. The samples used in this study were all single crystals grown by closed system CVT [72]. Plates parallel to natural faces were prepared by polishing, and ranged in thickness from 0.3 to 2.3 mm. All samples had nominal ruthenium concentrations of 0.1 mol%, and nominal tantalum concentrations of from 0 to 0.4 mol%.

All resistance measurements were performed by a two terminal technique. Circular contacts were evaporated onto the opposite faces of the plates. The contacts consisted of 500 Angstrom tantalum layers covered with 500 Angstroms of gold, onto which gold contacts were soldered using a Hughes Aircraft VTA-90 microsoldering unit. The tantalum layer reacts with the TiO_2 creating a heavily doped n-type layer under the contact. Tests on n-type TiO_2 samples showed that these contacts had low resistivities ($<0.1\ \Omega\,cm^2$). It was found however that the tantalum layer oxidises at around 400°C increasing the resistance of the contact. For this reason the measurements on the most conducting samples could not be continued above this temperature.

According to Cronemeyer [12], TiO_2 shows highly anisotropic conduction with $\sigma_c \gg \sigma_a$ below 850°C but is isotropic above this temperature. Hollander and Castro [95] found fully oxidised TiO_2 to be nearly isotropic however, and strong anisotropy only occurred in reduced samples. Even this anisotropy is suspect however since σ_c and σ_a were not measured in the same samples. In our samples the conductivity was measured perpendicular to the largest faces of the plates. The samples containing 0, 0.2 and 0.4 mol% tantalum were (100), (110) and (110) plates respectively, and the conductivity measured is therefore σ_a. The samples containing 0.1 mol% tantalum were (111) plates. The conductivity measured was therefore of mixed type in these samples, and given the actual dimensions of the plates and contacts, the current could have passed parallel to the c direction if this is more favourable. We found however that the measured conductivity of the samples can be accounted for without invoking anisotropic

conduction, and strong anisotropy as proposed by Cronemeyer would be incompatible with our results.

Results

The resistivities of the samples as a function of temperature are shown in Fig. 5.4.1. For comparison the resistivity of pure TiO_2, measured by Cronemeyer [12] perpendicular to the c-axis is also shown (dashed line). Axes of log resistivity and reciprocal temperature are used so that the slope of each curve is proportional to the total activation energy of the conduction process. The slope of the pure TiO_2 sample corresponds to an activation energy of 1.52 eV, and is due to the excitation of electrons from the valence to the conduction band.

The resistivity of the sample with no tantalum (curve 0) approaches that of pure TiO_2 at high temperature. At low temperature the resistivity is much lower, and the activation energy is low ($\approx$140 meV).

Curve 1, corresponding to a sample with 0.1% of both Ru and Ta is very similar to curve 0 in form. The resistivity of this sample is between 16 and 150 times lower than the sample without tantalum, but the activation energy is nearly the same at all temperatures.

Curve 1′, corresponding to a second sample with nominal Ru and Ta

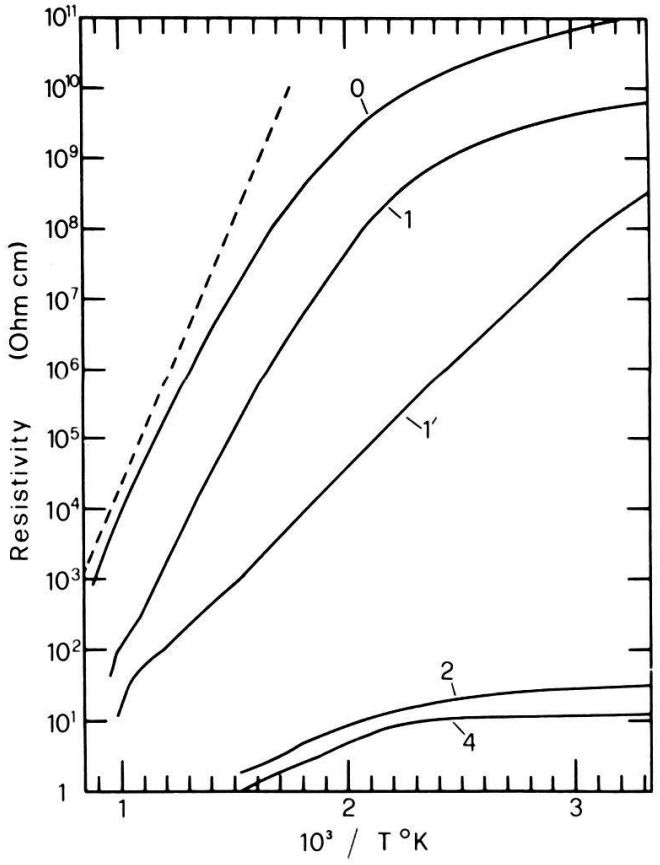

Figure 5.4.1
Electrical resistivity of TiO_2 doped with 0.1% Ru and various amounts of Ta. The labels give the nominal Ta to Ru concentration ratio. The dashed line shows the resistivity of pure TiO_2 from Ref. 12.

concentrations of 0.1%, is almost linear between room temperature and 1000 K. The activation energy is 0.62 eV in this range.

The samples with 0.2 and 0.4% Ta (curves 2 and 4) show very low resistivities (respectively 30 and 12 Ω cm) at room temperature. The temperature dependence is very weak in the range 300–400 K, but the resistivity decreases more sharply with increasing temperature above 400 K. In order to interpret our results we must consider the information available from our other investigations. From EPR and Mössbauer we know that the ruthenium in the crystal containing no tantalum is mostly Ru^{4+} but that some Ru^{3+} is present. Addition of tantalum converts the Ru^{4+} first to Ru^{3+}, and if the Ta:Ru concentration ratio is less than one then both Ru^{4+} and Ru^{3+} are present. If the Ta:Ru ratio is between one and two, then the ruthenium is present as Ru^{3+} and Ru^{2+}. For Ta:Ru ≥ 2 our optical results indicate that all ruthenium is present as Ru^{2+}, and an additional absorption band, similar to that of free carriers is present.

The conductivity of a semiconductor depends strongly on the position of the Fermi level in the band gap. In this case where ruthenium impurity states lie in the band gap, the conductivity will depend on the highest valence state of ruthenium present.

Our results show three distinct types of behaviour. If we suppose that the two samples with nominal Ta:Ru concentration ratios of one, have in fact ratios of just below one in one case (curve 1) and just above one in the other (curve 1′), and also that the crystal with a nominal Ta:Ru concentration ratio of two has a slightly higher ratio in reality, then we can divide our samples into three classes, corresponding to the types of behaviour.

i) $0 \leq$ Ta:Ru < 1. Highest valence state Ru^{3+}. This is the case for samples 0 and 1.
ii) $1 <$ Ta:Ru < 2. Highest valence state Ru^{2+}. This is the case for sample 1′.
iii) $2 <$ Ra:Ru. All ruthenium present as Ru^{2+}, but excess electrons present. This is the case for samples 2 and 4.

The samples having Ru^{3+} as the highest valence state show considerably higher resistivity at room temperature than the other samples, but lower resistivity than that measured for pure TiO_2 by Cronemeyer, and a low activation energy ($\approx$100 meV) at room temperature. The increase of activation energy with increasing temperature reflects the onset of transitions from the Ru^{3+} states to the conduction band. The optical absorption (Fig. 5.3.3) attributed to this process begins around one electron volt, but increases only slowly with energy up to 2.6 eV. At high temperatures the activation energy of conduction is close to 1.5 eV corresponding to intrinsic excitation of electrons from the valence band to the conduction band.

The conductivity of sample 1′, with Ru^{2+} as the highest valence state, shows an almost constant activation energy in the measured energy range, suggesting excitation of electrons from an impurity level to the conduction band. The activation energy is 0.62 eV, corresponding well to the sharp edge of the Ru^{2+} optical absorption band (Fig. 5.3.3).

The very low resistivities and activation energies of samples 2 and 4 are characteristic of n-type TiO_2 prepared by reduction [95] or by donor doping [42]. This effectively demonstrates that when all ruthenium is present as Ru^{2+}, further addition of donors is no longer compensated.

5.5. Photoelectron spectroscopy

We have studied the valence band density of states, and core level binding energies of pure and Ru doped TiO_2, using ultraviolet and X-ray photoelectron spectroscopy (UPS and XPS).

UPS has previously been applied to TiO_2 to investigate the valence band density of states, as well as the band gap surface states and variations in the position of the Fermi level with respect to the valence and conduction bands at the surface, as a function of surface stoichiometry [96, 97].

Core level spectroscopy has been extensively applied to ruthenium compounds in recent years. The binding energies of the core levels depend on the valence state of the ruthenium ion, and also on the presence of free carriers which shield the transition giving rise to doublets in some compounds of screened (lowered binding energy) and unscreened peaks. This technique has been applied notably to the pychlore oxides of ruthenium $M_2Ru_2O_7$ by Cox et al. [98] to demonstrate the metal to semiconductor transition in this family as a function of the metal M, and to ruthenium and ruthenium dioxide electrodes, enabling the chemical reactions involved in oxygen evolution and corrosion to be elucidated [99].

The depth in the sample from which photoelectrons may be emitted varies slightly with their kinetic energy, and on the materials being studied [100]. For both the UPS and XPS measurements discussed here the escape depth is about 2 nm. The depletion layer of a typical semiconductor is around 100 nm [101], and can be expected to be at least this wide in our samples in view of the high dielectric constant of rutile. The UPS and XPS spectra are therefore representative of the sample surface, and the position of the Fermi level in the band gap may be quite different from the position in the bulk if appreciable band bending occurs in the depletion zone.

UPS valence band spectra

Pure and Ru doped TiO_2 samples have been studied by photoelectron spectroscopy using HeI 21.2 eV illumination. The measurements were performed in a Kratos ES300 electron spectrometer equipped with a differentially pumped He discharge lamp, and with a base pressure of 10^{-10} Torr. The spectra were recorded at normal emission. From comparison of HeI and HeII spectra the three HeI satellite lines were each estimated to have 1.5% of the main line intensity, and the spectra were treated to remove their effect.

The samples examined were a pure TiO_2 (001) plate, cut from a Verneuil boule, and a TiO_2:2% Ru (111) single crystal face. The surfaces were examined after grinding with a hardened steel head, and after subsequent etching for five minutes using 4 keV Ar^+ ions. The surfaces examined were therefore polycrystalline and differences between the two samples due to the intrinsic anisotropy of TiO_2 [102] can be discounted. Freshly ground surfaces may be assumed to be nearly stoichiometric, whereas argon ion bombarded surfaces are strongly oxygen deficient.

Figure 5.5.1 shows the spectra of the pure and doped samples after grinding. The spectra have been aligned so that the centers of the valence band density of

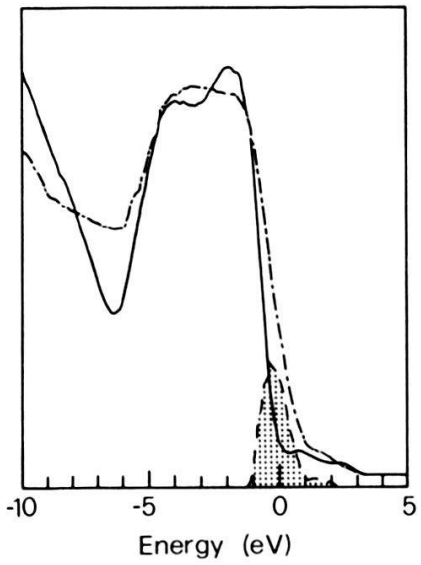

Figure 5.5.1
He(I) photoelectron spectra of ground TiO_2 (continuous line) and Ru doped TiO_2 (broken line) single crystals. The shaded region shows the difference between the spectra near the valence band summit.

states coincide, since the valence band structure should not be very sensitive to doping. The spectra are also normalised so that the total valence band intensities are the same in the two cases. The zero of energy has been placed at the summit of the valence band in the pure sample.

In the spectrum of the pure sample, the valence band structure extends to −6 eV, and the strong signal at lower energies arises from secondary electron emission. The double peak structure of the valence bands, and the low density of states in the band gap are characteristic of clean fully oxidised TiO_2 surfaces [97]. The Fermi level, established using a copper reference, is 3.2 eV above the valence band edge. The band gap is 3.05 eV so the Fermi level lies in the conduction band at the surface. From the insulating nature of the samples it is clear that in the bulk the Fermi level lies in the band gap. The bands therefore bend significantly downwards at the surface suggesting that even ground TiO_2 surfaces contain a certain number of donor defects.

The spectrum of the Ru doped sample shows some differences from that of the pure sample. The differences in the secondary electron emission will not be interpreted since this part of the spectrum is particularly sensitive to surface quality. The double peak structure of the valence band is absent, and the valence band edge appears to be shifted into the band gap. The difference between the density of states of the two spectra in the band gap is shown as the shaded region. The Fermi level is 3.4 eV above the intrinsic valence band edge. The resistivity of the samples [5.4] demonstrates that the Fermi level in the bulk is deep in the band gap, so this sample also has a strong negative band bending at the surface.

The main difference between the UPS spectra of the doped and pure sample are expected to come from the presence of the ruthenium 4d states in the band gap. The observed difference in the band gap density of states is too great, however, to come only from the d-electrons of the 2% of ruthenium present, taking into account the difference in the cross sections of the ruthenium 4d and oxygen 2p states at this photon energy. (The value of σ_{4d}/σ_{2p} is estimated to be ≈ 0.1, from the HeI spectrum of a pure RuO_2 sample.) It seems therefore that valence band broadening, perhaps due to poor surface quality must contribute to the observed difference. We may deduce however that if the Ru 4d states contribute to the spectrum, then they lie low in the band gap, or overlap the valence band summit.

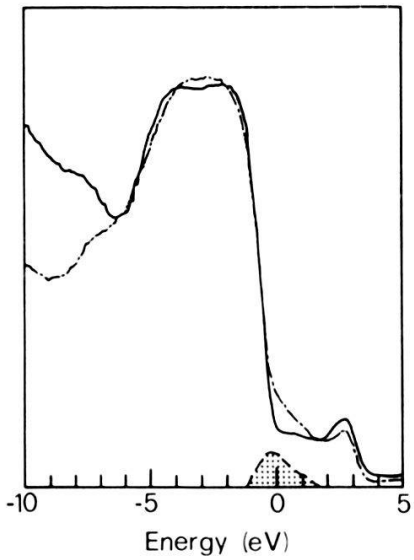

Figure 5.5.2
He(I) photoelectron spectra of pure (continuous line) and Ru doped (broken line) TiO_2 after argon ion etching. The shaded region shows the difference between the spectra near the valence band summit.

The spectra of the pure and doped samples after argon ion bombardment are shown in Fig. 5.5.2. In the spectrum of the pure sample the double peak structure of the valence band has disappeared. The band gap density of states has increased strongly and we note the appearance of a peak 0.3 eV below the conduction band edge. This spectrum is essentially identical to the Ar^+ bombarded TiO_2 spectra of Tait and Kasowski [97]. The Fermi level is 3.6 eV above the valence band summit. This shift with respect to the ground sample is due to increased downward band bending in the depletion zone produced by an increase in the number of donor centres at the surface. The peak near the conduction band edge is attributed to surface states associated with surface Ti^{3+} ions [103].

The valence band structure of the doped sample in Fig. 5.6.2 closely resembles that of the pure sample. A significant difference exists however in the band gap density of states. The doped sample also shows a peak near the conduction band edge which can be attributed to surface Ti^{3+} ions, but this peak is only weakly superimposed on the high density of states existing in the band gap. The difference between the pure and doped samples is shown as the shaded region in the lower half of the band gap. The Fermi level in this sample is not shifted by the Ar^+ bombardment, probably due to the ruthenium band gap states which compensate the surface donors.

XPS core level spectra

Ruthenium and titanium core level spectra have been measured on a TiO_2:2% Ru sample by X-ray core level photoelectron spectroscopy using 1253.6 eV MgKα radiation. The spectra were measured at room temperature in an Escalab 5 spectrometer with 5×10^{-11} Torr base pressure. The sample was mounted on a platinum tray, and was heated to around 1000°C in oxygen for three hours to clean the surface. Spectra were recorded after this treatment, and after two subsequent treatments, argon ion etching, and annealing in oxygen at around 650°C. The spectra have been calibrated using the Ti 2p binding energies of Göpel, Rocker and Feierabend for pure TiO_2 [104], and the Pt $4d_{5/2}$ line at 316 eV [105]. Good agreement was found between the two calibrations.

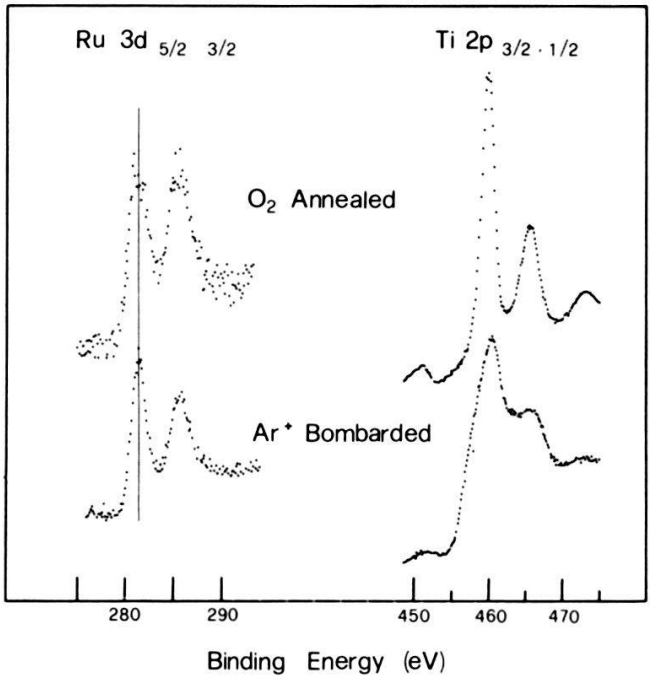

Figure 5.5.3
X-ray photoelectron spectra of Ru doped TiO_2 crystal showing ruthenium and titanium core level peaks.

Spectra taken after the high temperature treatment showed a very low ruthenium concentration at the surface due to formation of the volatile RuO_4, and will not be further discussed. The surface after argon ion etching is deficient in oxygen and can be compared to the argon bombarded surfaces studied by UPS. The effect of annealing in oxygen at 650°C is to restore surface stoichiometry, and the sample condition is comparable with the ground samples examined by UPS.

Figure 5.5.3 shows the Ti 2p and Ru 3d core level spectra obtained after annealing in oxygen, and after Ar^+ bombardment. The Ti 2p peak is a spin–orbit doublet, with a strong spin $\frac{3}{2}$ peak, and a weaker spin $\frac{1}{2}$ peak at higher binding energy. The Ru 3d peak is also a spin–orbit doublet, with a strong spin $\frac{5}{2}$ peak, and a weaker spin $\frac{3}{2}$ peak at higher energy. A comparison of Ru and Ti line intensities using the known cross sections [106] indicates a ruthenium concentration of 3% in the annealed sample, and 2% in the etched sample, in good agreement with the nominal value.

The Ti 2p spectrum of the sample annealed in oxygen shows a single doublet characteristic of Ti^{4+} which demonstrates that the surface is nearly stoichiometric. In comparison the spectrum after argon etching is broadened by the appearance of a second doublet at lower binding energy which can be attributed to Ti^{3+}. These results are essentially identical to those of Göpel et al. [104]. The UPS valence band spectra of the Ru doped TiO_2 sample (Fig. 5.5.2) also demonstrate the appearance of Ti^{3+} at the surface after argon ion bombardment.

In the Ru 3d spectra we observe after both treatments a single doublet with no indication of screening by free carriers. In the spectrum of the annealed sample the $\frac{3}{2}$ peak is enhanced by carbon contamination, the carbon 1 s peak in graphite being at 284.4 eV [105]. The $\frac{5}{2}$ peak is centred at 281.5 eV. After argon ion bombardment the $\frac{5}{2}$ peak remains at 281.5 eV. The $\frac{3}{2}$ peak is smaller and sharper, reflecting the removal of the carbon.

Table 5.5.1
Ruthenium $3d_{5/2}$ binding energies in non-metallic compounds.

Compound	Reference	Ru $3d_{5/2}$ (eV)	Valence state
RuO_4	107	283.3	VIII
RuO_3	107	282.5	VI
RuO_3	99	282.4	VI
$Y_2Ru_2O_7$	98	282.3	IV
$RuCl_3$	108	281.8	III
TiO_2:Ru	this work	281.5	II

The binding energies of the ruthenium core states vary with the electronic charge on the ion, and the position of the spin $\frac{5}{2}$ peak can therefore be used to estimate the valence state. In Table 5.5.1 we show the value obtained from our spectra, and the published values for the binding energy of this state in other compounds of ruthenium. Only non-metallic compounds are shown because of the strong shift due to screening by free electrons in metallic compounds [98]. The binding energy in our sample is below that of Ru^{3+} in $RuCl_3$, and we deduce that the valence state of the ruthenium is lower than three, although we know from Mössbauer [5.1] that the ruthenium in the bulk is Ru^{4+}. From our UPS spectra it is clear, however, that because of band bending in the depletion zone, the Fermi level at the surface is low in the conduction band. The situation at the surface is therefore comparable with a TiO_2:Ru sample that is donor doped until the Fermi level reaches the conduction band edge. Our previous studies [5.1, 5.3] indicate that in this case the ruthenium is present as Ru^{2+}. This would be consistent with the binding energies observed and we deduce that this is the valence state of the ruthenium ions at the surface of Ru doped TiO_2 samples.

Although argon ion etching removes oxygen from the surface leading to the formation of Ti^{3+}, our data indicates that the valence state of the surface ruthenium does not change.

In conclusion we have performed UPS and XPS measurements on Ru doped TiO_2 samples under conditions in which the surface is nearly stoichiometric, and then strongly reduced. Both sets of results are consistent with a strong downward bending of the bands in the depletion zone. From our UPS measurements we tentatively conclude that the occupied ruthenium 4d states lie low in the band gap, overlapping the valence band summit, as already inferred by optical and electrical measurements [5.3, 5.4]. From our XPS measurements we deduce that the ruthenium is stable at both the stoichiometric and reduced TiO_2 surface as Ru^{2+}.

5.6. Discussion

In Sections 5.1 to 5.5 we have presented a series of experiments with the aim of developing a coherent picture of the role played by ruthenium as an impurity in titanium dioxide. We summarise here the main conclusions which can be drawn from the results, and we propose an energy level scheme for ruthenium in TiO_2.

The Mössbauer measurements presented in Section 5.1 have shown that

nearly all the ruthenium in fully oxidised Ru doped TiO_2 is present as Ru^{4+}, substituting for Ti^{4+}. It was also possible to establish that the crystal field axis at the cation site lies along the principal axis of the octahedron formed by the six oxygen ions surrounding the cation, and to deduce the sign and strength of the electric field gradient. Experiments with crystals containing ruthenium and a small amount of tantalum ([Ta]/[Ru]<1) showed absorption peaks of both Ru^{4+} and Ru^{3+}, and other experiments showed that on addition of larger amounts of tantalum ([Ta]/[Ru]>1) the ion Ru^{2+} is formed. One advantage of Mössbauer spectroscopy is the selectivity of the measurements, which means that the spectra observed can be attributed without any doubt to one particular element, in this case ruthenium. A drawback of this technique is that high doping concentrations, of the percent level must be used to obtain good spectra.

EPR spectroscopy, as presented in Section 5.2, also allows different valence states of elements to be studied, and presents some advantages over Mössbauer spectroscopy in that it requires only very low doping levels and spectra are obtained much more rapidly. The greatest drawback of EPR is that only ions with magnetic moments can be observed. In this case only tri- and pentavalent ruthenium could be observed. In addition it is not possible to determine sufficiently accurately the population in a given valence state in order to estimate the populations in the other undetectable states. We have been able to show however that fully oxidised Ru doped titanium dioxide contains traces of both tri- and pentavalent ruthenium, and that a sample containing 0.1% of both ruthenium and tantalum, and likewise a sample without tantalum but reduced in hydrogen at 500°C, contained significant concentrations of Ru^{3+} ions. The spectra also showed that this ion is present on undisturbed cation sites. Although spectra of many different elements may be close or even superimposed in EPR, identification of ruthenium spectra is unambiguous because of the characteristic ^{99}Ru and ^{101}Ru hyperfine interactions.

Optical absoprtion spectroscopy, as presented in Section 5.3 offers the possibility of measuring the energies of transitions involving ruthenium ions in various valence states. Identification of the species responsible for a given transition requires a thorough knowledge of the system, however, and it is only with the information available from Mössbauer and EPR that it has been possible to attribute the observed absorption bands to ruthenium ions in particular valence states, and therefore to deduce the transitions involved. The spectra obtained allow us to estimate the energies of the different valence states of ruthenium with respect to the conduction (CB) and valence (VB) bands of TiO_2 (Fig. 5.6.1).

The electrical measurements presented in Section 5.4 demonstrate the influence of ruthenium on the electrical conductivity of TiO_2. We see that not only is ruthenium doped TiO_2 insulating at room temperature, but that addition of donors no longer leads to a marked increase in conductivity as is the case for pure TiO_2. This is consistent with the compensating behaviour of ruthenium as deduced from Mössbauer and EPR measurements. The activation energies of conduction found for the samples containing tri- and divalent ruthenium confirm the conclusions drawn from the optical measurements as to the positions of these states in the band gap.

In Section 5.5 we present photoelectron spectroscopy of pure and ruthenium doped TiO_2 samples. These measurements are sensitive only to the first atomic layers of the sample surface, where the situation may be different from that in the

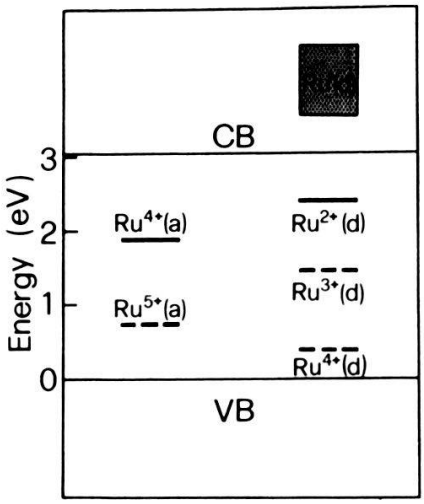

Figure 5.6.1
Schematic energy level diagram for Ru in TiO_2, showing the conduction band (CB), valence band (VB), and the proposed ruthenium donor (d) and acceptor (a) levels. The levels which have been precisely determined are indicated by solid lines. The levels which are approximate are indicated by broken lines.

bulk if significant band bending occurs at the surface. We have found the Fermi level of both pure and ruthenium doped titanium dioxide to lie low in the conduction band, implying a significant downward bending of the bands. This fact is compatible with the XPS evidence which shows that the ruthenium at the surface of Ru doped TiO_2 is present as Ru^{2+}.

We propose in Fig. 5.6.1 a schematic energy level diagram for ruthenium donor and acceptor levels in titanium dioxide. The donor level (d) of the $n+$ ion is defined with respect to the conduction band (CB) by the energy necessary for the transition:

$$Ru^{n+} \xrightarrow{h\nu} Ru^{(n+1)+} + e^{-}(CB)$$

This level can also be called the $Ru^{n+/(n+1)+}$ level. The acceptor level (a) of the $n+$ ion is defined with respect to the valence band by the energy neccessary for the transition:

$$Ru^{n+} \xrightarrow{h\nu} Ru^{(n-1)+} + h^{+}(VB)$$

This level can also be called the $Ru^{n+/(n-1)+}$ level.

In general the Ru^{n+}(a) level lies above the $Ru^{(n-1)+}(d)$ level by an amount which corresponds to the stabilisation of the additional electronic charge by lattice polarisation.

The fact that addition of donors to ruthenium doped titanium dioxide leads to free carrier formation before Ru^{+} appears means that the $Ru^{+}(d)$ level is a resonant state lying above the bottom of the conduction band. The $Ru^{2+}(d)$ level is placed 0.6 eV below the conduction band from both optical and electrical evidence. For the Ru^{3+} ion, the onset of optical absorption associated with the donor transition is not sharp, and this donor level is therefore approximate. The fact that some pentavalent ruthenium has been observed by EPR in rutile, presumably to compensate trivalent impurities, indicates that the $Ru^{4+}(d)$ level lies above the valence band edge, although no direct observation exists allowing this level to be placed precisely. The Ru^{4+} acceptor level is placed 1.9 eV above the valence band edge corresponding to the onset of optical absorption associated with this transition. The $Ru^{5+}(a)$ level also lies in the band gap since it must lie above the $Ru^{4+}(d)$ level.

In conclusion the experiments reported in this chapter present a coherent picture of the role of ruthenium as an impurity in titanium dioxide. It is shown that the stable valence state of ruthenium in fully oxidised TiO_2 is Ru^{4+}, and that on addition of donors or on reduction, the transitions to tri- and divalent ruthenium occur. Optical and electrical evidence shows that free carriers are formed rather than Ru^{+} on strong doping with donors. The influence of the compensating behaviour of ruthenium on the optical, electrical and photoelectrical properties of TiO_2 has been investigated, and the results can be interpreted in terms of the energy level scheme shown in Fig. 5.6.1.

6. Conclusions

We have prepared and studied single crystals in the system $Ti_{1-x}Ru_xO_2$. Three distinct crystal types are found depending on the relative concentrations of titanium and ruthenium. For $x \leqslant 0.02$ (2 mol% RuO_2) single phase, insulating crystals are obtained with the rutile structure and lattice parameters close to those of pure titanium dioxide. For $x \geqslant 0.98$ (98 mol% RuO_2) single phase, metallic crystals are obtained with lattice parameters close to those of pure ruthenium dioxide. For intermediate concentrations a highly ordered, two phased system is found where the two phases have compositions close to the pure oxides, and have the same orientation with a coherent interface. These two phased crystals have bulk resistivities of around $10^4\ \Omega$ cm with 3% RuO_2, and become good metals for higher ruthenium concentrations.

On the ruthenium rich side of the system we have studied samples of pure ruthenium dioxide, and ruthenium dioxide containing 2 mol% titanium dioxide. The optical reflectivity of the sample containing titanium is the same as that of the pure sample within experimental uncertainty, and we deduce that the presence of 2% titanium produces no significant change in the number of carriers, nor in the band structure near the Fermi level. Electrical measurements have shown that the titanium impurities scatter the conduction electrons in RuO_2, leading to significant differences between the residual resistivity ratios of pure and doped samples.

The main part of this study is devoted to the characterisation of the single phased crystals with less than 2% ruthenium dioxide. Several techniques were used and allow the following conclusions to be drawn: Ruthenium replaces Ti^{4+} substitutionally in rutile as Ru^{4+}, and therefore behaves neither as an acceptor, nor as a donor. If trivalent (acceptor) impurities are present these are compensated by the ruthenium which becomes pentavalent. If pentavalent (donor) impurities are present these are also compensated by the ruthenium which becomes trivalent or even divalent, depending on the relative concentrations of the ruthenium and the donors. The effect of these valence changes on the optical properties of the system are spectacular since each valence state from tetravalent to divalent contributes a characteristic band to the absorption spectrum of the system. The compensating behaviour of ruthenium has an important influence on the electrical properties of rutile. In the absence of ruthenium the addition of small quantities of a donor impurity increases dramatically the electrical conductivity of the system. In ruthenium doped titanium dioxide a marked increase in conductivity on addition of donors only occurs after all the ruthenium has been reduced to the divalent state. The conducting properties of mixed TiO_2–RuO_2

films used primarily in electrochemistry can certainly be attributed to conduction in the ruthenium dioxide phase, rather than to an increase in the conductivity of titanium dioxide due to the incorporation of ruthenium.

It is hoped that this work provides a clear description of the role of titanium in ruthenium dioxide, and of ruthenium in titanium dioxide, which may serve as a reference in future studies of the TiO_2–RuO_2 system in thin film or ceramic form.

Acknowledgments

We have presented here a summary of a large amount of experimental work which has been performed on single crystals in the system TiO_2–RuO_2. The crystal growth has been performed exclusively in this laboratory, and some of the crystals studied were prepared by H. Berger.

Many of the experiments have been performed in other laboratories, and I would like to express my thanks to Professor F. E. Wagner of Munich for Mössbauer, Dr K. W. Blazey of IBM Zürich for EPR, Dr R. Kötz of Brown Boveri, Baden for UPS, Dr R. Egdell of Imperial College London for XPS, and Dr Ph. Buffat and Dr P. Stadelmann of the Institute of Electron Microscopy of the EPFL for electron microscopy.

A certain amount of experimental work has been performed in this laboratory, and I gratefully acknowledge the collaboration of C. A. Georg, and the excellent technical assistance of H. Jotterand and J. Lambercy.

My thanks are also due to the people without whom this project would not have existed. and who have guided and financed it, my director Dr F. Lévy, the Professor of the Institut of Applied Physics E. Mooser, Dr C. Schuler, Dr A. Menth and Dr S. Stucki of Brown Boveri, Baden, and the "Credit pour l'Encouragement de la Récherche Scientifique", Switzerland.

REFERENCES

[1] R. T. Atanasowski, *Symp. Electrocatalysis*, Neunkirchen (1983).
[2] R. Kötz, *Symp. Electrocatalysis*, Neunkirchen (1983).
[3] T. Kawai and T. Sakata, *Chem. Phys. Letts 72*, 87 (1980).
[4] S. Trasatti and G. Lodi, *Electrodes of Conductive Metallic Oxides, Part A*, Elsevier Scientific Publishing Co., Amsterdam, p. 301 (1980).
[5] L. F. Mattheiss, Phys. Rev. *B 13*, 2433 (1976).
[6] W. H. Baur and A. A. Khan, Acta Cryst. *B 27*, 2133 (1971).
[7] O. W. Johnson, Phys. Rev. *136*, A284 (1964).
[8] N. Daude, C. Gout and C. Jouanin, Phys. Rev. *B 15*, 3229 (1977).
[9] J. L. Jourdan, C. Gout and J. P. Albert, Solid State Comm. *31*, 1023 (1979).
[10] S. Hüfner and G. K. Wertheim, Phys. Rev. *B 8*, 4857 (1973).
[11] D. W. Fischer, Phys. Rev. *B 5*, 4219 (1972).
[12] D. C. Cronemeyer, Phys. Rev. *87*, 876 (1952).
[13] J. Pascual, J. Camassel and H. Mathieu, Phys. Rev. Letts. *39*, 1490 (1977).
[14] H. Mathieu, J. Pascual and J. Camassel, *18*, 6920 (1978).
[15] M. Cardona and G. Harbeke, Phys. Rev. *137*, A1467 (1965).
[16] F. Arntz and Y. Yacoby, Phys. Rev. Letts. *17*, 857 (1966).
[17] A. Frova, P. J. Boddy and Y. S. Chen, Phys. Rev. *157*, 700 (1967).
[18] K. Vos and H. J. Krusemeyer, Solid State Comm. *15*, 949 (1974).
[19] K. Vos and H. J. Krusemeyer, J. Phys. *C 10*, 3893 (1977).

[20] A VON HIPPEL, J. KALNAJS and W. B. WESTFAL, J. Phys. Chem. Solids *23*, 779 (1962).
[21] V. M. ARUTYUNYAN, A. O. ARAKELYKYAN, G. A. KUBATOV, ZH. R. PANOSYAN, A. G. SARKISYAN, K. K. SIDORIN and YU. V. SHMARTSEV, Sov. Phys. Solid State *25*, 543 (1983).
[22] J. RIGA, C. TENRET-NOËL, J. J. PIREAUX, R. CAUDANO and J. J. VERBIST, Physica Scripta *16*, 351 (1977).
[23] J. RUDOLPH, Z. Naturf. *14a*, 727 (1959).
[24] P. F. CHESTER, J. Appl. Phys. *32*, Suppl., 2233 (1961).
[25] P. I. KINGSBURY, W. D. OHLSEN and O. W. JOHNSON, Phys. Rev. *175*, 1091 (1968).
[26] L. N. SHEN, O. W. JOHNSON, W. D. OHLSON and J. W. DE FORD, Phys. Rev. *B 10*, 1823 (1974).
[27] J. B. WACHTMAN, S. SPINNER, W. S. BROWER, T. FRIDIGER and R. W. DICKSON, Phys. Rev. *148*, 811 (1966).
[28] L. A. K. DOMINIK and R. K. MACCRONE, Phys. Rev. *156*, 910 (1967).
[29] L. A. K. DOMINIK and R. K. MACCRONE, Phys. Rev. *163*, 757 (1967).
[30] T. R. SANDIN and P. H. KEESOM, Phys. Rev. *177*, 1370 (1969).
[31] J. KERSSEN and J. VOLGER, Physica *69*, 535 (1973).
[32] D. C. CRONEMEYER, Phys. Rev. *113*, 1222 (1959).
[33] V. N. BOGOMOLOV, E. K. KUDINOV, D. N. MIRLIN and YU. A. FIRSOV, Sov. Phys. Solid State *9*, 1630 (1968) and *9*, 2502 (1968).
[34] V. N. BOGOMOLOV and D. N. MIRLIN, Phys. Stat. Sol. *27*, 443 (1968).
[35] D. N. MIRLIN, I. I. RESHINA and L. S. SOCHAVA, Sov. Phys. Solid State *11*, 1995 (1970).
[36] P. F. CHESTER, J. Appl. Phys. *32*, 866 (1961).
[37] H. P. R. FREDERIKSE, J. Appl. Phys. *32*, Suppl. 2211 (1961).
[38] J. H. BECKER and W. R. HOSLER, J. Phys. Soc. Japan *18*, Suppl, 152 (1963).
[39] J. H. BECKER and W. R. HOSLER, Phys. Rev. *137*, A1872 (1965).
[40] R. G. BREKENRIDGE and W. R. HOSLER, Phys. Rev. *91*, 793 (1953).
[41] R. R. HASIGUTI, K. MINAMI and H. YONEMITSU, J. Phys. Soc. Japan *16*, 2223 (1961).
[42] N. P. BOGORDITSKII, V. KRISTYA and YA. I. PANOVA, Sov. Phys. Solid State *9*, 187 (1967).
[43] A. H. KAHN, H. P. R. FREDERIKSE and J. H. BECKER, *Proc. Buhl. Int. Conf. Transition Metal Compounds*, Pittsburgh (1963).
[44] E. K. KUDINOV, D. N. MIRLIN and YU. A. FIRSOV, Sov. Phys. Solid State *11*, 2257 (1970).
[45] H. J. GERITSEN, S. E. HARRISON, H. R. LEWIS and J. P. WITTKE, Phys. Rev. Letts. *2*, 153 (1959).
[46] K. MIZUSHIMA, M. TANAKA and S. IIDA, J. Phys. Soc. Japan *32*, 1519 (1972).
[47] P. O. ANDERSON and E. L. KOLLBERG, Phys. Rev. *B 8*, 4956 (1973).
[48] O. W. JOHNSON, W. D. OHLSEN and P. I. KINGSBURY, Phys. Rev. *175*, 1102 (1968).
[49] J. P. WITTKE, J. Electrochem. Soc. *113*, 193 (1966).
[50] M. GUERMAZI, G. MAREST, A. PEREZ, B. D. SAWICKA, J. A. SAWICKI, P. THEVENARD and T. TYLISZCZAK, Mat. Res. Bull. *18*, 529 (1983).
[51] D. ZWINGEL, Solid State Commun. *20*, 397 (1976).
[52] D. ZWINGEL, Solid State Commun. *26*, 775 (1978).
[53] G. G. STONE and L. A. BURSILL, Phil. Mag. *15*, 1397 (1977).
[54] A. K. GOEL, G. SHORINKO and F. H. POLLAK, Phys. Rev. B *24*, 7342 (1981).
[55] J. E. GRAEBNER, E. S. GREINER and W. D. RYDEN, Phys. Rev. B *13*, 2426 (1976).
[56] S. M. MARCUS and S. R. BUTLER, Physics Letters *26A*, 518 (1968).
[57] W. D. RYDEN, A. W. LAWSON and C. C. SARTAIN, Phys. Rev. B *1*, 1494 (1970).
[58] V. M. LEBEDEV, YU. E. ROGINSKAYA, N. L. KLIMASENKO, V. I. BYSTROV and YU. N VENEVTSEV, Russ. J. Inorg. Chem. *21*, 1380 (1976).
[59] B. SH. GALYAMOV, YU. E. ROGINSKAYA, R. R. SHIFRINA and YU. N. VENEVTSEV, Sov. Phys. Solid State *20*, 1291 (1978).
[60] YU. E. ROGINSKAYA, B. SH. GALYAMOV, I. D. BELOVA, R. R. SHIFRINA, V. B. KOZHEVNIKOV and V. I. BYSTROV, Elektrokhimiya *18*, 1327 (1982).
[61] W. A. GERRARD and B. C. H. STEELE, J. Appl. Electrochem. *8*, 417 (1977).
[62] YU. E. ROGINSKAYA, V. I. BYSTOV and D. M. SHUB, Russ. J. Inorg. Chem. *22*, 110 (1977).
[63] B. SH. GALYAMOV, S. M. EMEL'YAMOV, YU. E. ROGINSKAYA and YU. N. VENEVTSEV, Sov. Phys. Solid State *20*, 129 (1978).
[64] YU. E. ROGINSKAYA, B. SH. GALYAMOV, V. M. LEBEDEV, I. D. BELOVA and YU. N. VENEVTSEV, Russ. J. Inorg. Chem. *22*, 273 (1977).
[65] M. VALIGI and D. GAZZOLI, Z. Phys. Chem. Neue Folge 125, 89 (1981).
[66] H. SCHAFER, *Chemical Transport Reactions*, Academic Press (1964).
[67] F. IZUMI, H. KODAMA and A. ONO, J. Cryst. Growth *47*, 139 (1979).

[68] G. D. DARTYVAN, Sov. Phys. Crystallogr. *21*, 499 (1976).
[69] T. NIEMYSKI and W. PICKARCZYK, J. Cryst. Growth *1*, 177 (1967).
[70] F. ROSENBERGER, M. C. DELONG and J. M. OLSON, J. Cryst. Growth, *19*, 317 (1973).
[71] Y. S. HUANG, H. L. PARK and F. H. POLLAK, Mat. Res. Bull. *17*, 1305 (1982).
[72] P. TRIGGS, H. BERGER, C. A. GEORG and F. LÉVY, Mat. Res. Bull *18*, 677 (1983).
[73] P. GROSSE, *Freie Elktronen in Festkörpern*, Springer-Verlag, Berlin (1979).
[74] L. COLQUITT, J. Appl. Phys. *36*, 2454 (1965).
[75] C. A. GEORG, P. TRIGGS and F. LÉVY, Mat. Res. Bull. *17*, 105 (1982).
[76] M. W. SHAFER, R. A. FIGAT, B. OLSEN, S. J. LAPLACA and J. ANGILELLO, J. Electrochem. Soc. *126*, 1624 (1979).
[77] H. SCHÄFER, G. SCHNEIDEREIT and W. GERHARDT, Z. Anorg. Allgem. Chem. 319, 327 (1963).
[78] D. S. RODBELL, J. M. LOMMEL and R. C. DEVRIES, J. Phys. Soc. Jpn *21*, 2430 (1969).
[79] D. B. ROGERS, R. D. SHANNON, A. W. SLIEGHT and J. L. GILLSON, Inorg. Chem. *8*, 841 (1969).
[80] P. GILBART, Compt. Rend. *261*, 1525 (1965).
[81] P. GÜTLICH, R. LINK and A. TRAUTWEIN, *Mössbauer Spectroscopy and Transition Metal Chemistry*, Springer-Verlag, Heidelberg (1978).
[82] F. E. WAGNER and U. WAGNER, *Mössbauer Isomer Shifts*, eds G. K. Shinoy and F. E. Wagner, North Holland Pub. Co., Amsterdam (1978).
[83] O. C. KISTER and A. H. LUMPKIN, Phys. Rev. *C. 13*, 1132 (1976).
[84] G. KAINDL, W. POTZEL, F. E. WAGNER, U. ZAHN and R. L. MÖSSBAUER, Z. Physik *226*, 113 (1969).
[85] F. E. WAGNER, R. WORDEL, P. TRIGGS and F. LÉVY, to be published.
[86] M. VALIGI, D. CORDISCHI, D. GAZZOLI, K. P. KEIJZERS and A. KLASSEN, to appear in J. C. S. Faraday Trans. I.
[87] A. RAIZMAN, J. T. SUSS and S. SZAPIRO, Solid State Comm. *9*, 1799 (1971).
[88] K. W. BLAZEY, K. A. MÜLLER, W. BERLINGER, P. TRIGGS and F. LÉVY, to appear in Solid State Commun.
[89] J. E. GEUSIC, M. PETER and E. O. SCHULTZ du BOIS, Bell System Technical J. *38*, 291 (1959).
[90] P. SALVADOR, C. GUTIERREZ, P. TRIGGS and F. LÉVY, Mat. Res. Bull. *19*, 643 (1984).
[91] C. GUTIÉRREZ and P. SALVADOR, to appear in J. Electroanal. Chem.
[92] K. W. BLAZEY and H. WEIBEL, J. Phys. Chem, in press.
[93] K. MIZUSHIMA, M. TANAKA, A. ASAI, S. IIDA and J. B. GOODENOUGH, J. Phys. Chem. Solids *40*, 1129 (1979).
[94] J. GAUTRON, J. F. MARUCCO and P. LEMASSON, Mat. Res. Bull. *16*, 575 (1981).
[95] L. E. HOLLANDER and P. L. CASTRO, Phys. Rev. *119*, 1882 (1960).
[96] V. E. HENRICH, G. DRESSELHAUS and H. J. ZEIGER, Phys. Rev. Letts. *36*, 1335 (1976).
[97] R. H. TAIT and R. V. KASOWSKI, Phys. Rev. *B 20*, 5178 (1979).
[98] P. A. COX, R. G. EGDELL, J. B. GOODENOUGH, A. HAMNETT and C. C. NAISH, J. Phys. C 16, 6221 (1983).
[99] H. J. LEWERENZ, S. STUCKI and R. KÖTZ, Surf. Sci. 126, 463 (1983).
[100] A. W. CZANDERNA, Methods and Phenomena 1, Elsevier, Amsterdam (1975).
[101] S. R. MORRISON, *Electrochemistry at Semiconductor and Oxidised Metal electrodes*, Plenum, New York (1980).
[102] V. E. HENRICH and R. L. KURTZ, Phys. Rev. *B 23*, 6280 (1981).
[103] V. E. HENRICH, G. DRESSELHAUS and H. J. ZEIGER, Solid State Commun. *24*, 623 (1977).
[104] W. GÖPEL, G. ROCKER and R. FEIERABEND, Phys. Rev. B 28, 3427 (1983).
[105] Handbook of X-Ray Photoelectron Spectroscopy, Perkin–Elmer, Minnesota (1979).
[106] S. EVANS, R. PRITCHARD and J. THOMAS, J. Electron. Spec. Related Phenomena 14, 341 (1978).
[107] K. S. KIM and N. WINOGRAD, J. Catalysis *35*, 66 (1974).
[108] B. FOLKESSON, Acta Chem. Scand. *27*, 287 (1973).